Plume-ridge interactions: Ridge ~~suction~~-ward versus plate ~~-~~drag plume flow

Fengping Pang[1], Jie Liao[1,2,3], Maxim D. Ballmer[4], Lun Li[1,2,3]

[1]School of Earth Sciences and Engineering, Sun Yat-Sen University, Guangzhou 510275, China

[2]Guangdong Provincial Key Lab of Geodynamics and Geohazards, Guangzhou 510275, China

[3]Southern Marine Science and Engineering Guangdong Laboratory (Zhuhai), Zhuhai 519000, China

[4]Department of Earth Sciences, University College London, London, United Kingdom

Correspondence: Jie Liao (liaojie5@mail.sysu.edu.cn)

Abstract

~~Mid~~The analysis of mid-ocean ridges and hotspots that are sourced by deep-rooted mantle plumes ~~are two attractive windows to allow~~allows us to get a glimpse of mantle structure and dynamics. Dynamical interaction between ridge and plume processes have been widely proposed and studied, particularly in terms of ridge ~~suction.~~-ward plume flow. However, the effects of plate drag on ~~plumes~~plume-lithosphere and plume-ridge interaction ~~remains~~remain poorly understood. ~~Quantification of suction versus plate drag between ridges and plumes remains absent.~~ In particular, the mechanisms that control plume flow towards vs. away from the ridge have not yet been systematically studied. Here, we use 2D thermomechanical numerical models ~~to study the~~of plume-ridge interaction~~, exploring~~ to systematically explore the effects of (i) ~~the~~ridge spreading rate ~~of ridge~~, (ii) ~~the~~initial plume head radius, and (iii) ~~the~~ plume-ridge distance ~~systematically~~. Our numerical

experiments suggest two different geodynamic regimes: (1) plume ~~motion-prone to~~flow towards the ridge ~~suction~~ is favored by strong buoyant mantle plumes and small plume-ridge distances; (2) plume drag away from the ridge is in turn promoted by fast ridge spreading, at least for small-to-intermediate plumes. We find that the pressure gradient between the buoyant plume and ~~short plume-ridge distance, and (2) plume migration driven by~~spreading ridge at first drives ridge-ward flow, but eventually the competition between plate drag ~~is promoted by fast-ridge spreading rate.~~and the gravitational force of plume flow along the base of the sloping lithosphere controls the fate of plume (spreading towards vs. away from the ridge). Our results highlight that fast-spreading ridges exert strong plate dragging force, ~~rather than suction on plume motion,~~ which sheds new light on ~~the~~ natural observations of largely absent plume ~~absence~~ lithosphere interaction along ~~the~~ fast-spreading ridges, such as the East Pacific ~~Rises~~Rise.

1 Introduction

Mid-ocean ridges (MORs) and hotspots are two main regions for deep material recycling to the surface of the Earth. However, these two units are not always isolated but showing strong interactions in some cases, termed as plume-ridge interaction (Morgan, 1971). Of up to 50 mantle plumes revealed by seismic tomography (French and Romanowicz, 2015; Montelli et al., 2004), more than 20 plumes are found to be associated with nearby ridges (Ito et al., 2003). The plume ridge interaction is manifested by some geophysical and geochemical anomalies along ridge axis, e.g., high mantle potential temperature (Dalton, 2014), enriched radiogenic isotopes towards ridge axis (Cushman et al., 2004; Douglass and Schilling, 1999; Yang et al. 2017), and the lineament of volcanoes on the seafloor (Geissler et al., 2020; Lénat and Merle, 2009). Besides, plumes may also promote migration of MORs (Müller and Roest, 1998; Mittelstaedt et al., 2008, 2011;Whittaker et al., 2015), which was evidenced by successive ridge jumps towards mantle plumes, e.g., Hawaii, Amsterdam (Li and Detrick, 2003). The major factors affecting ridge suction on plumes includes ridge spreading rate, plume buoyancy flux and their spatial distance (Fig. 1b; François et al., 2018; Kincaid et al., 1996; Ribe et al., 1995; Ribe, 1996; Sleep, 1997). Most plume-ridge interaction systems links to slow-spreading ridges (< 2.5 cm/yr; Gerya, 2012) and small mantle plumes and short plume-ridge distances. However, systematical studies investigating these parameters remain scarce regarding the effects of these parameters on the behavior of plume-ridge interaction.

Additionally, among the interacted systems, plumes interacting with ridges appear more abundant near the Mid-Atlantic ridge (MAR), comparing to the East Pacific Rise (EPR). The reason attributed to such a distribution is still enigmatic. A previous study (Jellinek et al., 2003) proposed that fast-spreading ridges

56

1 Introduction

Mid-ocean ridges (MORs) and hotspots are two main regions for deep material recycling to the surface of the Earth. However, these two units are not always isolated, but rather show strong interactions in some cases, termed as plume-ridge interaction (Morgan, 1978). Of up to 50 mantle plumes revealed by seismic tomography (French and Romanowicz, 2015; Montelli et al., 2004), more than 20 plumes are found to be associated with nearby ridges (Fig.1a; Ito et al., 2003). Plume-ridge interaction is manifested by geophysical and geochemical anomalies along the ridge axis, e.g., high mantle potential temperature (Dalton et al., 2014), enriched radiogenic isotope anomalies (Cushman et al., 2004; Douglass and Schilling, 1999; Yang et al. 2017), and adjacent lineations of seamounts (Ballmer et al., 2013b; Geissler et al., 2020; Lénat and Merle, 2009). Furthermore, plumes may promote migration of MOR spreading centers (Müller et al., 1998; Mittelstaedt et al., 2008, 2011; Whittaker et al., 2015), as evidenced by successive ridge jumps towards mantle plumes, e.g., at Iceland, Amsterdam-Saint Paul and Galapagos hotspots (Hardarson et al., 1997; Maia et al., 2011; Mittelstaedt et al., 2012). The interaction dynamics of a ridge with an on-axis and off-axis plume has been widely studied and modeled in analogue and numerical experiments, revealing that the major controlling factors involve the ridge spreading rate, plume buoyancy flux and their spatial distance (François et al., 2018; Ito et al., 1997; Kincaid et al., 1996; Ribe et al., 1995; Ribe, 1996; Sleep, 1997). Indeed, most plume-ridge interaction systems are associated with slow-spreading ridges and small mantle plumes and short plume-ridge distances (Fig.1b). However, numerical studies systematically investigating the effects of these parameters on plume-ridge interaction and quantify the controlling forces remain scarce.

As has been noted previously, buoyant plumes tend to spread ridge-ward along the sloping base of the lithosphere (Morgan, 1978; Schilling, 1991; Small, 1995). Regions of divergent mantle flow beneath MORs represent the lowest dynamic-pressure regions in the oceanic asthenosphere, and thus tend to suck ambient asthenospheric and plume materials towards the spreading center (Niu, 2014). On the other hand, the viscous drag at the base of the plate tends to convey the spreading plume material away from the MOR (Ribe and Christensen, 1994, 1999). Indeed, plume spreading at the base of the lithosphere is governed by the competition of trench-ward viscous plate drag vs. ridge-ward gravitational and pressure-driven forces (Kincaid et al.,1996). These gravitational and tectonic forces compete with other to control the regime of plume-ridge interaction, but their balance remains to be quantified.

The distribution of hotspots with classified as plume-ridge interaction (ridge-ward spreading) vs. no interaction (plate-drag spreading) also still remains enigmatic. Plume-ridge interaction is much more common near the Mid-Atlantic ridge (MAR) than near the East Pacific Rise (EPR) (Fig. 1a). Near the EPR, only the Pukapuka and Sojourn ridges display clear evidence of ridge-ward flow of the magmatic source, but these volcanic ridges have been attributed to a horizontally propagating viscous finger or small-scale convection, and not a mantle plume (Ballmer et al., 2013b; Clouard and Bonneville, 2005; Harmon et al., 2011). A previous study (Jellinek et al., 2003) proposed that fast-spreading ridges ~~exert strong suction on plumes and attract the surrounding plumes entirely from deep depth (Fig. 1c), resulting in the absence of plumes adjacent to the EPR (Fig. 1a). However, a series of spatiotemporal volcanic chains with linear progressing age are found in different Oceans (Jackson et al., 2010). Not only do MORs suck the proximal plumes into the spreading center (Koptev et al., 2015; Niu, 2014), but they can conversely drag mantle plumes away. Therefore, an alternative explanation~~

~~to the plume absence along the fast spreading ridges could be plate drag, i.e., fast spreading ridges push away the surrounding plumes. Plate drag, in contrast to suction, however, remains poorly studied. Moreover, either ridge suction or plate drag acts on mantle plumes remains an intriguing question.~~

~~This study utilizes two-dimensional (2D) numerical models~~guide upwelling mantle flow towards the spreading center to convey the surrounding plumes from deep depth entirely into the MOR melting zone (Fig. 1c), resulting in the absence of hotspots adjacent to the EPR (see also Rowley et al., 2016; Rowley and Forte, 2022). However, fast plate spreading also tends to drag mantle plumes away from the MOR (Kincaid et al., 1995, 1996), leading to the typically parabolic shapes of hotspot swells such as near Hawaii (Ribe and Christensen, 1994). Whether the increased spreading rates in the Pacific vs. Atlantic promote ridge-ward vs. plate-drag plume flow remains an intriguing question.

The principal goal of this study is to investigate the process of plume-ridge interaction, with ~~emphasizing~~an emphasis on the effects of model parameters on the ridge ~~suction versus plate drag. We demonstrate that ridge suction and~~-ward vs. plate-drag ~~on plumes are influenced by the distinctive parameters. Slow spreading rate, short distance and large plume radius promote ridge suction, whereas the opposite~~plume spreading. We explore the effects of ~~these~~various model parameters ~~favor pushing plumes away. We further propose that fast spreading ridges exerts strong dragging on plumes due to~~ , such as the ~~large shear force along the base~~size of the ~~oceanic plate. This process of plate drag, instead of~~plume, ridge ~~suction, on plume may support the explanation of the~~spreading rate, and plume-ridge distance. Finally, we use our model results to interpret the difference of natural plume-ridge interaction ~~absence along~~systems in different oceans, particularly the striking difference between the East Pacific ~~Rise.~~ and Atlantic in this regard.

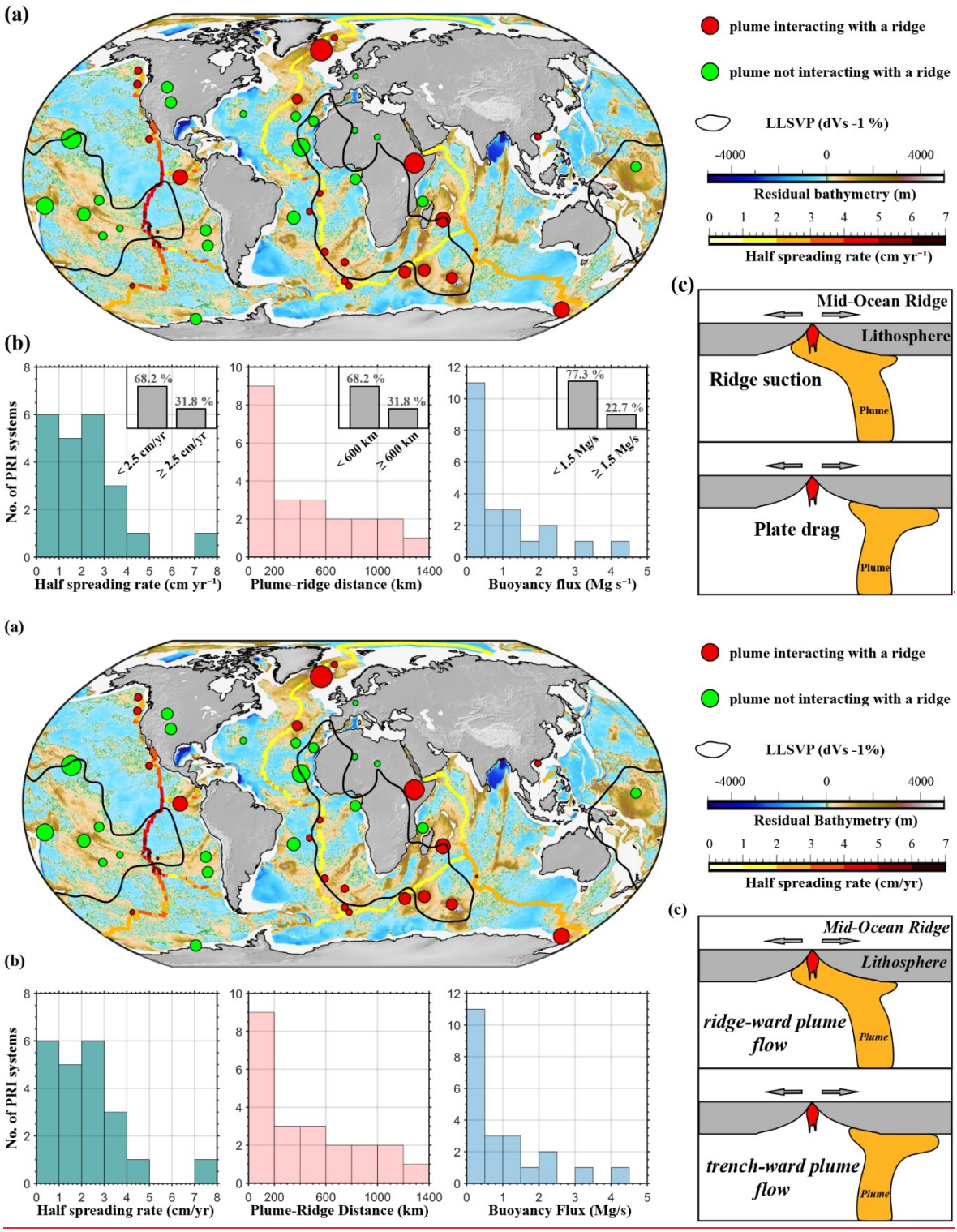

Figure 1. Global plume-ridge interaction systems. **(a)** Global distribution of mid-ocean ridges and mantle plumes. Residual bathymetry of the ocean basins come from Straume et al. (2019). Mid-ocean ridges are painted in color solid lines corresponding to half-spreading rate. Plumes not interacting with a ridge are shown by green circles, and hotspots linked to ridges are in red dots (Ito et al., 2003); size

refers to the plume buoyancy flux from Hoggard (2020). Black lines denote the regions of two LLSVPs under the South Africa and Pacific Ocean (Torsvik et al., 2006). **(b)** Histograms of influential factors of plume-ridge interaction systems. ~~**Figure 1.** Global plume-ridge interaction systems. **(a)** Residual bathymetry of the ocean basins (Straume et al., 2019). Mid-ocean ridges are painted in color solid lines corresponding to half-spreading rate. Plumes not interacting with a ridge are shown by green circles, and hotspots linked to ridges are in red dots (Ito et al., 2003), and size refers to the plume buoyancy flux from Hoggard (2020). Black lines denote the regions of two LLSVPs under the South Africa and Pacific Ocean (Torsvik et al., 2006). **(b)** Histograms of influential factors of plume-ridge interaction systems. Half spreading rate and plume-ridge distance come from Gplates~~Half spreading rate and plume-ridge distance is taken from GPlates (Müller et al., 2016; Whittaker et al., 2015). Plume-ridge interaction systems link to slow-spreading ridge and small mantle plumes and short plume-ridge distance. **(c)** Sketches of ridge~~ suction~~-ward (top panel) and plate~~ ~~-drag plume flow (bottom panel) mode proposed, respectively.

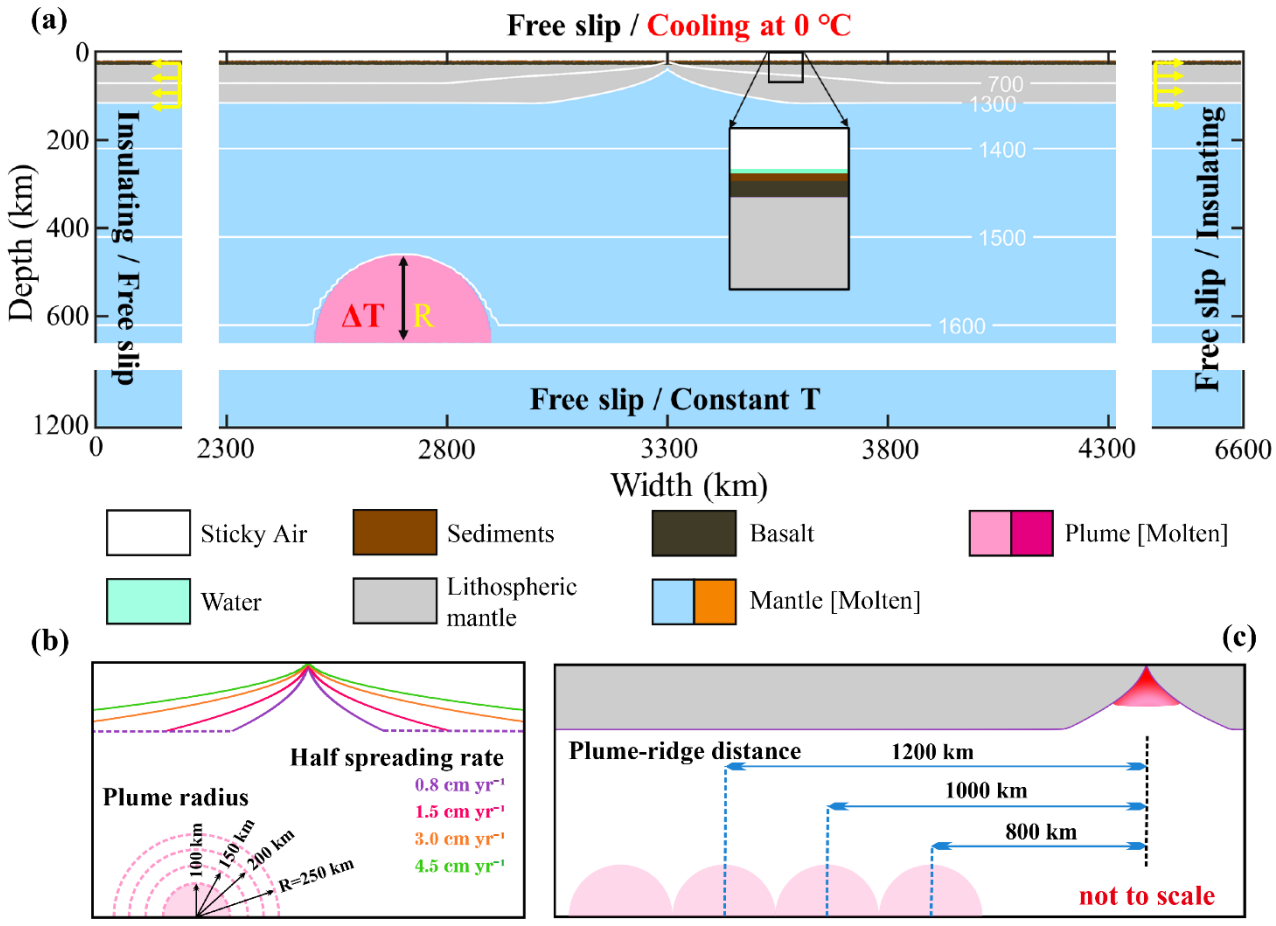
(a)
Free slip / Cooling at 0 °C
Depth (km)
0
200
400
600
1200
Insulating / Free slip
Free slip / Insulating
700
1300
1400
1500
1600
ΔT
R
Free slip / Constant T
0
2300
2800
3300
3800
4300
6600
Width (km)
Sticky Air
Sediments
Basalt
Plume [Molten]
Water
Lithospheric mantle
Mantle [Molten]
(b)
Half spreading rate
0.8 cm yr⁻¹
1.5 cm yr⁻¹
3.0 cm yr⁻¹
4.5 cm yr⁻¹
Plume radius
100 km
150 km
200 km
R=250 km
(c)
Plume-ridge distance
1200 km
1000 km
800 km
not to scale

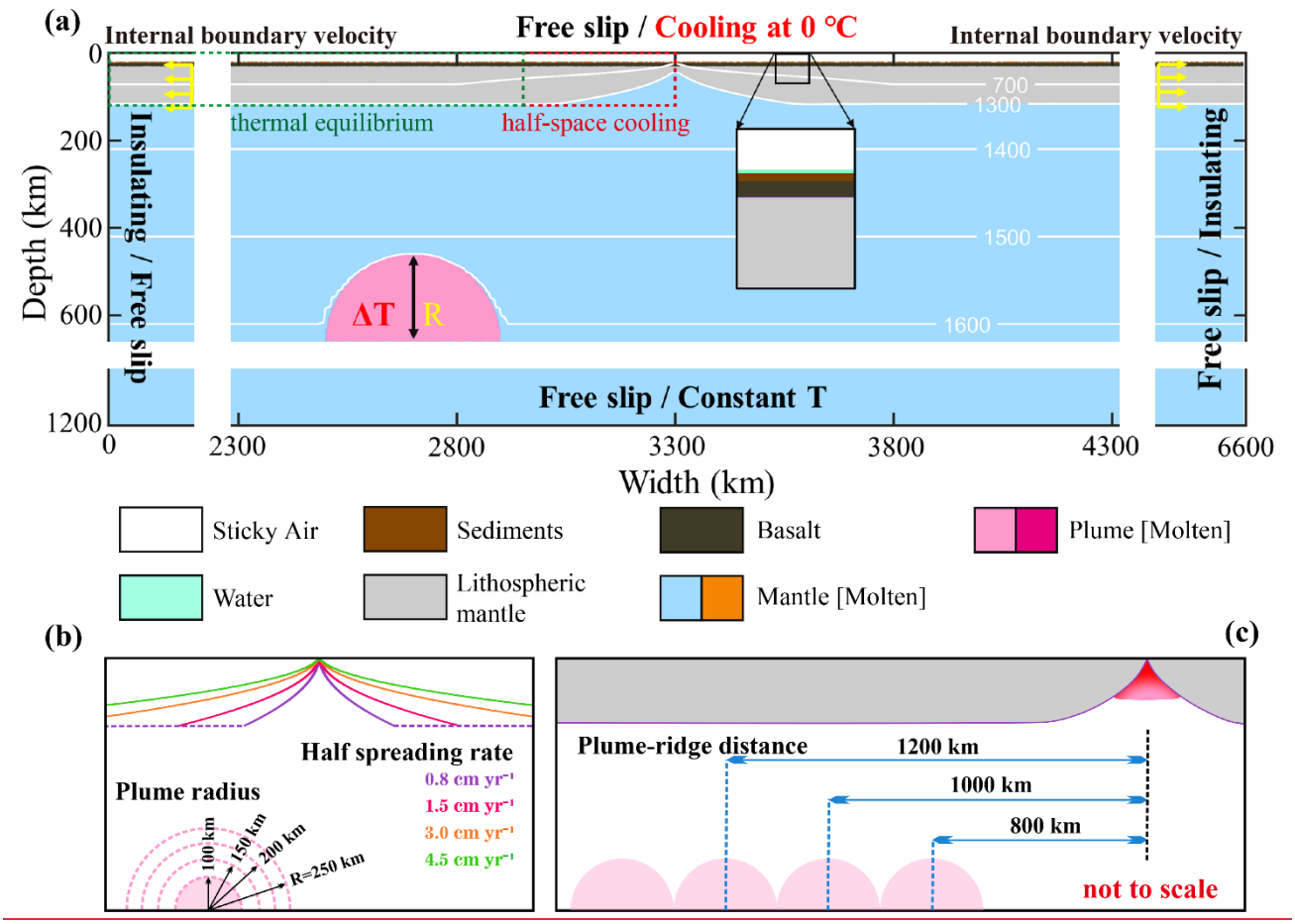

Figure 2. Model setup. **(a)** Initial composition and boundary conditions. The oceanic plate consists of half-space cooling part and the thermal equilibrium part. A 50-Myrs-old mid-ocean ridge sets in the middle of the model based on half-space cooling temperature structure. A thermal and chemical anormal mantle plume locates at 660 km. ~~Colored boxes refer to~~ Different colors indicate the initial rock ~~type,~~types and corresponding newly formed molten rock types. Yellow arrows are ~~also show~~the half-spreading rates imposed internal in the ~~rock boxes~~lithosphere (i.e., from 20 km to 120 km in depth) to simulate ridge spreading. **(b)** Initial tested ridge and plume configurations. **(c)** Initial tested plume-ridge distances.

2 Numerical modelling

2.1 Modelling methods

~~We~~To explore plume-lithosphere and plume-ridge interaction, we conduct numerical simulations ~~by~~ utilizing the 2D thermo-mechanical ~~coupled codes~~code I2VIS, which is based on staggered finite difference method combined with marker-in-cell techniques (Gerya and Yuen, 2003, 2007). This modeling framework uses both Eulerian ~~grid~~grids and ~~fully~~ randomly-distributed Lagrangian markers to jointly solve equations of conservation of mass, momentum and energy (Eq. (1)-(3), respectively):

$$\nabla \cdot \vec{v} = 0 \qquad (1)$$

$$\frac{\partial \sigma'_{ij}}{\partial x_j} - \frac{\partial P}{\partial x_i} + \rho g_i = 0 \qquad (2)$$

$$\rho C_p \left(\frac{DT}{Dt}\right) = -\nabla \cdot \vec{q} + H_r + H_a + H_s + H_l \qquad (3)$$

where v refers to the velocity, σ'_{ij} the deviatoric stress tensor, P the pressure, ρ the density, g the gravity acceleration, $\frac{D}{Dt}$ the Lagrangian time derivative, C_p the heat capacity, and ~~$\vec{q}$~~q the heat flux. Additionally, H_r, H_a, H_s, and H_l are the radioactive, adiabatic, shear, and latent heat productions, respectively.

We employ ~~the~~a non-Newtonian visco-plastic rheology (Gerya and Yuen, 2007) in the models. The viscous rheology depends on ~~the~~ stress ~~rate~~, temperature and pressure~~, and can be~~. The appropriate viscosity is expressed ~~by the effective viscosity~~ as that of ~~the~~a composite diffusion and dislocation-creep material (Eq. (4)).

$$\frac{~~1~~}{~~\eta_{eff}~~} \frac{1}{\eta_{vis}} = \frac{1}{\eta_{diff}} + \frac{1}{\eta_{disl}} \qquad (4)$$

in which η_{diff} and η_{disl} are the diffusion and dislocation creep viscosity, respectively, and can be further computed as Eq. (5) and Eq. (6):

$$\eta_{diff} = \frac{1}{2} A \sigma_{crit}^{1-n} \exp\left(\frac{PV_a + E_a}{RT}\right) \qquad (5)$$

$$\eta_{disl} = \frac{1}{2} A^{\frac{1}{n}} \dot{\varepsilon}_{II}^{\frac{1-n}{n}} \exp\left(\frac{PV_a + E_a}{nRT}\right) \qquad (6)$$

where P is the pressure, T is the temperature, $\dot{\varepsilon}_{II}$ is the second invariant of the strain rate tensor, σ_{crit} is the diffusion-dislocation creep transition stress, and A–, E_a, V_a, and n are the strain rate pre-exponential ~~factor~~factor, activation energy, activation volume, and stress exponent, respectively. The plastic behavior η_{pla} is described by the Drucker-Prager yield criterion (Byerlee, 1978; Ranalli, 1995) according to Eq. (7) and Eq. (8):

$$\sigma_y = C + P\varphi \quad (7)$$

$$\eta_{pla} = \frac{\sigma_y}{2\dot{\varepsilon}_{II}} \quad (8)$$

in which σ_y ~~as~~is the yield stress, C is the rock cohesion and φ is the effective friction coefficient. The effective viscosity η_{eff} of rocks is thus constrained by ~~all abovementioned~~ both viscous and plastic deformation, where the rheological ~~laws in our models.~~behavior depends on the minimum viscosity attained between ductile and brittle fields:

$$\eta_{eff} = \min(\eta_{vis}, \eta_{pla}) \quad (9)$$

Partial melting, melt extraction and percolation ~~to the base of the crust~~ are also considered ~~and completed~~in the model in a simplified way (Gerya, 2013). ~~In the model, the melt extraction and percolation is modeled indirectly and considered as an instantaneous process. We calculate the melt fraction (i.e. without melt extraction), M_0, of the mantle based on a nonlinear parameterized batch melting model of Katz (2003). For other lithologies, the melt fraction (M_0) are assumed to increase linearly with temperature and are calculated as Eq. (8~~The melt fraction (M_0) of the crust are assumed to increase with temperature and are calculated according to Eq. (10):

$$M_0 = 0 \text{ when } T \le T_{solidus}$$

$$M_0 = \frac{(T - T_{solidus})}{(T_{liquidus} - T_{solidus})} \text{ when } T_{solidus} < T < T_{liquidus} \quad (~~8~~10)$$

$$M_0 = 1 \text{ when } T \ge T_{liquidus}$$

~~Where~~where $T_{solidus}$ and $T_{liquidus}$ are the solidus and liquidus temperature of different rock ~~type~~types, respectively~~.~~, taken from Katz et al. (2003).

In our model, melt extraction is modeled indirectly and considered as an instantaneous process (Gerya et al., 2015). The extracted melt is assumed to move vertically from the molten source and then added to the bottom of the crust. Partial melt is extracted from the mantle and instantaneously displaced to the bottom of the crust and converted into hot mafic magma, obeying the conservation of material.

The amount of extracted melt during the evolution of each experiment is traced by the ~~lagrangian~~Lagrangian markers (Gerya, 2013). The total amount of melt, M, for every marker ~~takes into~~excludes the amount of previously extracted melt according to Eq. (~~9~~):11):

$$M = M_0 - \Sigma_n M_{ext} \quad (~~9~~11)$$

where $\Sigma_n M_{ext}$ refers to the total melt fraction extracted during the previous n melt extraction timesteps. ~~Rocks are assumed non molten if the extracted melt fraction ($\Sigma_n M_{ext}$) surpasses the standard melt fraction ($\Sigma_n M_{ext} > M_0$). The modeled melt is extracted upwards when the total amount of melt M exceeds the given extraction threshold M_{min} = 2wt %. Hence, the extracted melt is assumed to move vertically instantaneously from the molten source and then added to the bottom of the crust.~~

The effective density of mafic magma and molten crust depends on its melt fraction and is calculated as (Gerya et al., 2015; Gülcher et al., 2020):

$$\rho_{eff} = \rho_{solid}(1 - M + M\frac{\rho_{0,molten}}{\rho_{0,solid}}) \quad (12)$$

where $\rho_{0,molten}$ and $\rho_{0,solid}$ are the reference densities of the molten and solid crust. ρ_{solid} is the crust density at given pressure and temperature, which can be computed as:

$$\rho_{solid} = \rho_{0,solid}[1 - \alpha(T - 298)][1 + \beta(P - 0.1)] \quad (13)$$

with thermal expansion $\alpha = 3 \times 10^{-5} K^{-1}$ and compressibility $\beta = 10^{-11} Pa^{-1}$.

Surface processes, such as erosion and sedimentation, are considered by solving the transport equation on the Eulerian nodes at each time step (Gerya and Yuen, 2003). Our erosion/sedimentation model uses gross-scale erosion/sedimentation rates which are independent of local elevation and topography (Burov and Cloetingh, 1997). We use constant and moderate rates of erosion (0.315 mm/yr) and sedimentation (0.0315 mm/yr), respectively, which falls within naturally observed ranges.

2.2 Model setup

The ~~initial~~size of the model ~~dimensions are set as~~ box is 6600 × 1200 km, with a nonuniform grid of 501 × 301 computational nodes in length and depth, respectively (Fig. 2). ~~We use a variable~~The densest grid ~~spacing, so as to reach a higher grid resolution~~is located in the ~~middle part~~center of the model domain (i.e., grid size decreases linearly from 20 km at the edges to 2 km at the ridge axis), where ~~the~~ plume-ridge interaction would happen. The model consists of a 20 km thick sticky air layer ~~fitting~~to accommodate crustal surface deformation~~, an oceanic lithosphere and asthenosphere till depth of 660 km.~~. To reproduce the oceanic lithosphere, we choose a typical layered model ~~from the uppermost mantle to the surface, and~~, where the ~~crustal part of this lithosphere~~crust is composed of a water level (2 km), a sediment layer (1.5 km), and a basalt layer (7.5 km). The oceanic lithosphere and asthenosphere in the model are both ~~modelled~~modeled as dry olivine (the different colors for the mantle lithosphere and asthenosphere in the figures of this paper are only for better visualization). Besides, a 50-Myrs-old mid-ocean ridge is set on central part of the lithosphere, splitting the model domain into two parts. At the depth of 660 km, a 200-km-wide semicircular plume is located on the left of model domain, corresponding to the onset of plume-ridge interaction from the mantle transition zone.

Detailed rock parameters are listed in ~~Tabel~~Table 1.

~~The thermal conditions of the top and bottom boundaries are fixed at 273 and 2513 K, respectively. The left and right boundaries are both insulating, with no external heat flow across them. The temperature configuration of the oceanic lithosphere is interpolated with a linear gradient constrained by constant temperatures of 273 and 1573 K at the top and bottom of the lithosphere. Below the oceanic lithosphere, an adiabatic temperature gradient of 0.5 K km^{-1} is applied. In terms of ridge, the thermal structure and thickness of the lithosphere are calculated by the infinite half-space cooling formulation (Turcotte and Schubert, 2014). The hot plume is set an excess temperature of 250 K to trigger a thermal-compositional plume rising from the model box. All the velocity boundaries are free slip boundaries. An additional velocity is imposed on both sides of the ridge to represent the half spreading rate.~~

~~Tabel~~The thermal conditions at the top and bottom boundaries are fixed at 273 and 2513 K, respectively. The left and right boundaries are both insulating, with no external heat flow across them. The initial temperature structure of the mantle is adiabatic (0.5 K km^{-1}), which results in a temperature at 660 km depth of 1843 K. The initial temperature structure of the oceanic plate consists of half-space cooling part and thermal equilibrium part (Fig. 2a). The half-space cooling model is used to describe the oceanic plate younger than 50 Myr, and the thermal equilibrium structure is used to describe older oceanic parts. In other words, the thermal age of the lithosphere far away from the ridge is fixed at 50 Myr with a constant plate thickness (i.e., ~100 km). The hot plume is set a circular thermal and compositional (see Table 1) anomaly with an excess temperature of 250 K to trigger a rising thermochemical plume. All the velocity boundaries are free slip boundaries. Additional internal

boundary velocities are imposed at 500 km from each side boundary in the lithosphere to maintain the imposed half spreading rate (Fig. 2a).

Table 1. Rock physical properties used in the numerical models.

Parameters	Sediments	Ocean Crust	Mantle	Plume	Reference [a]
Flow law	Wet quartz	Basalt	Dry olivine	Wet olivine	
Preexponential factor A(Pa^{n}s)	1.97×10^{17}	4.80×10^{22}	3.98×10^{16}	5.01×10^{20}	1
Activation energy E_a(KJ mol^{-1})	154	238	532	470	1
Activation volume V_a(J bar^{-1}mol^{-1})	0	0	1	0.8	1
Exponent n	2.3	3.2	3.5	4	1
Cohesion C(Pa)	2×10^{7}	2×10^{7}	2×10^{7}	2×10^{7}	1
Effective friction coefficient φ	0.6/0.3	0.6/0.3	0.6/0.3	0.6/0.3	1
Density ρ(Kg m^{-3})	2600	3000	3300	3270	2
Radioactive heating H_r(W m^{-3})	2×10^{-6}	2.2×10^{-7}	2.2×10^{-8}	2.5×10^{-8}	2

a: 1-(Ranalli, 1995), 2-(Turcotte and Schubert, 2014)

Other physical parameters used for all rocks include: gas constant R=8.314 J K^{-1}mol^{-1}, thermal expansion α=3×10^{-5} K^{-1}, compressibility β=1×10^{-11} Pa^{-1}, heat capacity Cp=1000 J kg^{-1}K^{-1}.

3 Model Results

We conduct a series of numerical experiments to investigate ridge suction versus plate drag acts on plumes. The ~~effect~~effects of three major model parameters (i.e., the spreading rate of mid-ocean ridge, the initial plume head radius, and the plume-ridge distance) ~~has been~~are systematiclly studied. The typical dynamic evolution of models with ridge ~~suction and~~-ward vs. plate--drag ~~on plumes~~plume flow are demonstrated.

3.1 ~~Ridge suction dominated model~~Model evolution

~~In~~ **with ridge** ~~suction dominated models, the rising plume flows toward the spreading ridge as a result of ridge suction, and~~**-ward plume flow**

For models with dominant ridge-ward flow, the typical model evolution is shown in Fig. 3 (the major model parameters used in this case are: the half spreading rate of 8 mm yr^{-1}, the initial plume head radius of 200 km, and the off-axis distance of 800 km). In the early plume head stage, the buoyant mantle plume rises up rapidly in a mushroom-like shape (Fig. 3b) and ~~thus~~ imposes dynamic stresses at the base of the overriding oceanic plate, leading to significant surface uplift~~. (Figs.~~ (Fig. 3a ~~b~~). The ascending plume experiences ~~intensive~~extensive decompression melting ~~along~~at the base of the overriding plate, and due to the dynamic overpressure, spreads laterally, forming two branches that flow in opposite directions ~~with uplifted elevation~~ (Fig. 3c). ~~Along with~~A large amount of plume ~~spreading, the overriding~~material is eventually entrained towards the spreading center, ponding underneath the ridge axis, and significantly affecting the ridge dynamics. The entrainment of hot plume material promotes decompression melting (Figs. 3d, e) and increases the temperature beneath the ridge (Fig. S2). Within the overlying lithosphere, the buoyant mantle plume leads to stress localization and strongly weakens the oceanic plate ~~begins to drag both plume branches away from the ridge. On the~~

~~other hand,~~(Figs. S1, S3). As the plume eventually flows upward along the increasingly sloping base of the plate ~~divergence at~~near the MOR~~ creates a dominant~~, massive melting and crust production occurs (Fig. S1), forming an oceanic plateau of thickened crust. In addition to this gravitational force that guides plume material of the right branch ridge-ward, plate spreading drags both branches in the opposite direction. Moreover, convective and tectonic stresses ("plume push" and "ridge suction ~~effect.~~") affect both branches of the plume in a different way. As a consequence, the two branches evolve asymmetrically: the right branch that flows ~~toward~~towards the ridge axis is more vigorous than the left branch, and the plume tail is also tilted towards the spreading center (Figs. ~~3c-e).~~3c-e). For a more detailed discussion of the underling controlling forces, see below.

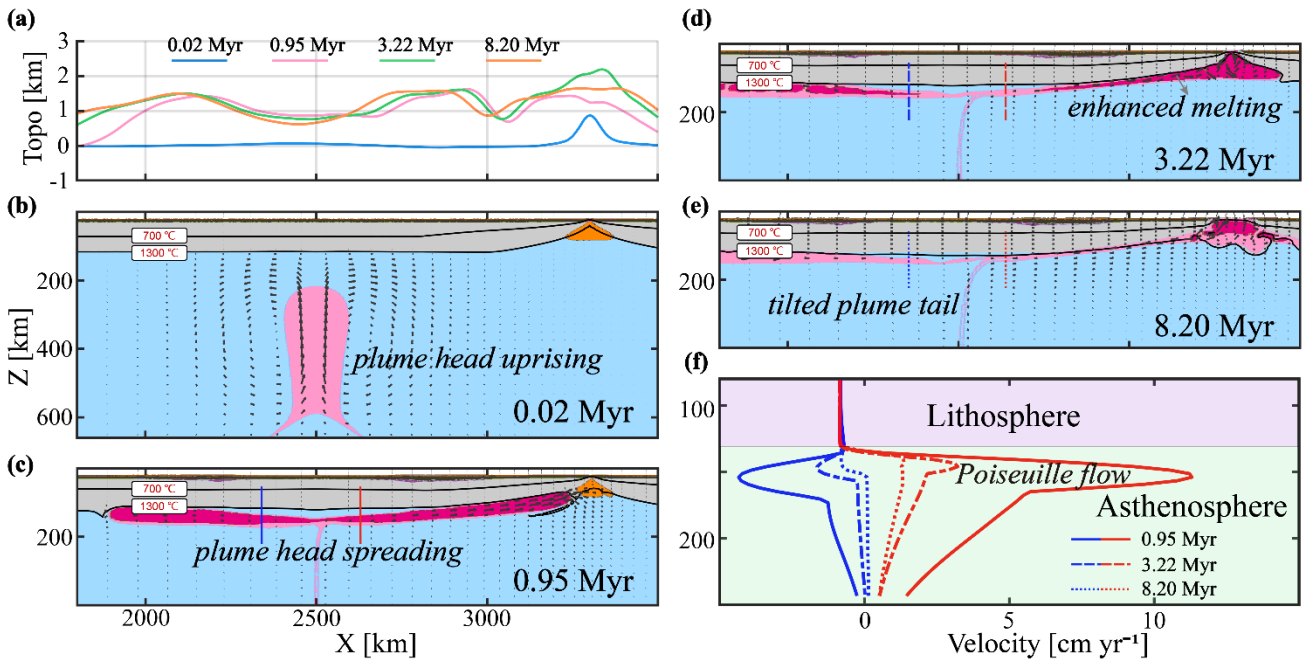

Figure 3. The evolution of the reference model M12 (see Table S1 in supplementary material) with dominant ridge-ward plume flow. The main model parameters employed in this case are: half spreading rate of 8 mm yr^{-1}, an initial plume head radius of 200 km, and an off-axis distance of 800 km. **(a)** surface topography over time along the flow path. **(b-e)** Snapshots of composition for the reference

model (M12). **(f)** Profiles of the horizontal velocity component over time at the sections as indicated (color-coded) in panel (c-e).

The mantle flow ~~vertical~~horizontal velocity profiles (Fig. 3f) further demonstrate the ~~dominant effect~~dominance of ridge~~-suction on~~-ward plume ~~head spreading. Figure 3f shows~~flow, showing that plume flow is faster towards the spreading ridge than away from it. The velocity profiles elucidate dominant Poiseuille flow, with the maximum flow velocities in the middle of the ~~flowing layer, decreasing upwards and downwards.~~asthenospheric channel. Such velocity profiles are well consistent with ~~the~~observations of seismic anisotropy~~ observation~~ at the Reunion plume (Barruol et al. 2019). The branches of the spreading plume head move significantly faster than the overriding plate~~ moves slower than the ponding plume, and hence~~. Therefore, plate drag actually slows down the spreading of the plume branches~~. Without suction effect from~~ in this model case. Because of the asymmetrical spreading ~~center,~~of the ~~left~~ plume ~~branch flows out much slower than~~ head, the buoyancy flux carried by the right branch of the plume (density anomaly multiplied by horizontal velocity from Figure 3f) is also much larger than that carried by the left branch.

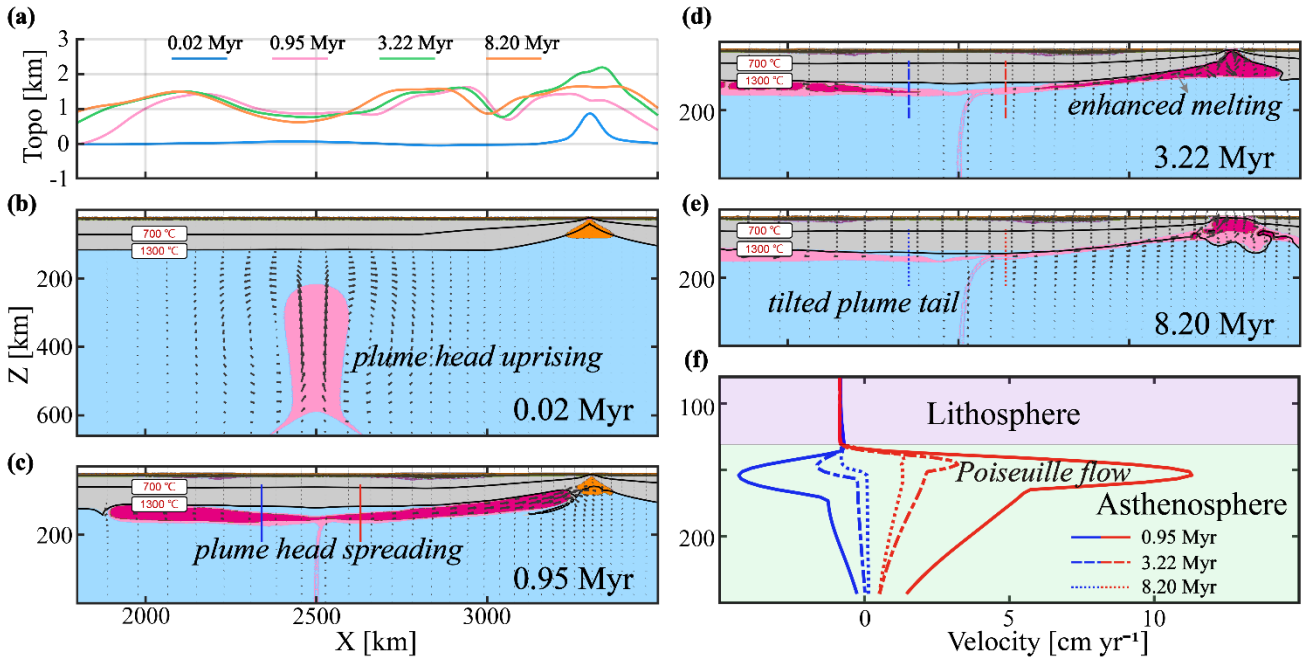

Figure 3. Reference model evolutions of ridge suction on plume flow. **(a)** topography evolutions along the flow path of selected snapshots. **(b-e)** snapshots of reference suction dominated model in compositional domain. Solid, dash and dotted lines are the velocity profiles of plume branches 100 km aside the plume stem and plot in (f). **(f)** mantle flow velocity structure evolutions of ridge-ward and dragged plume domains marked in red and blue lines, respectively.

A large amount of plume material is entrained towards the spreading center, ponding underneath the ridge axis, and significantly affecting the ridge dynamics. The entrainment of hot plume material increases the temperatures beneath the ridge, promotes decompression melting and boosts surface heat flux (Fig. 5d). The buoyant mantle plume then strongly weakens the overlying oceanic plate and changes the stress state of the overlying oceanic plate, forming a series of tension cracks due to the forced uplift (Figs. 5c,d). Magma extracts to the surface through these cracks, especially in areas that lithosphere is thin and weak. As such, a large amount of plume material beneath the thinner lithosphere near the mid-ocean ridge is extracted to the surface, which depends on the melt temperature and

~~pressure. Such melt extraction via separated tension cracks may imply the formation of near linear volcanic ridges.~~

3.2 ~~Plate-drag dominated model~~ Model evolution with plate-drag plume flow

~~In plate-drag dominated~~For models~~, the rising mantle~~ with dominant plume ~~is simulated to~~ flow away from the ~~spreading~~ ridge ~~and is dominantly driven by~~("plate-drag flow"), the ~~drag of the moving plate (~~typical model evolution is shown in Fig. ~~4). This~~ 4. The controlling parameters of the representative model ~~has a similar configuration as the ridge suction dominated model (~~shown in ~~Fig. 3)~~Figure 4 are the same as for the model shown in Figure 3, except ~~with~~for a smaller radius (100 km) and ~~interacts with a~~ faster spreading ~~center~~ridge (half spreading rate: 45 mm yr^{-1}). ~~The~~ At first, the ascending plume head spreads out similarly as in the case described above and interacts with the overriding oceanic ~~plate~~lithosphere. The largest surface uplift is ~~produced~~sustained just above the plume head (Fig. 4a), slightly different from the previous model in which the highest surface elevation is observed on ~~the two~~both sides of the plume conduit (Fig. 3a). Related to this spreading and uplift, divergent stresses are sustained in the overlying lithosphere (Fig. S4), but no weakening or yielding occurs (Fig. S6). The plume head ~~spreads laterally underneath the oceanic plate, and~~ undergoes significant decompression melting near the deflection point (Fig. 4c). ~~Unlike the ridge suction dominated model, in which a large portion of plume material flows towards the ridge~~However, thick and cold lithosphere prevents magma from extracting (Fig. S4). As the plume cools, partially molten plume gets solidified speedily (Figs. 4d-e and S5). In contrast to the reference model from section 3.1, this model displays most plume material flowing away from the ridge ~~owing~~, likely due to ~~the dragging~~

~~of~~dominant plate drag (Figs. 4c-e). ~~–~~Indeed, the left branch of the plume consistently displays larger buoyancy fluxes and maximum velocities than the right side over time (Fig. 4f).

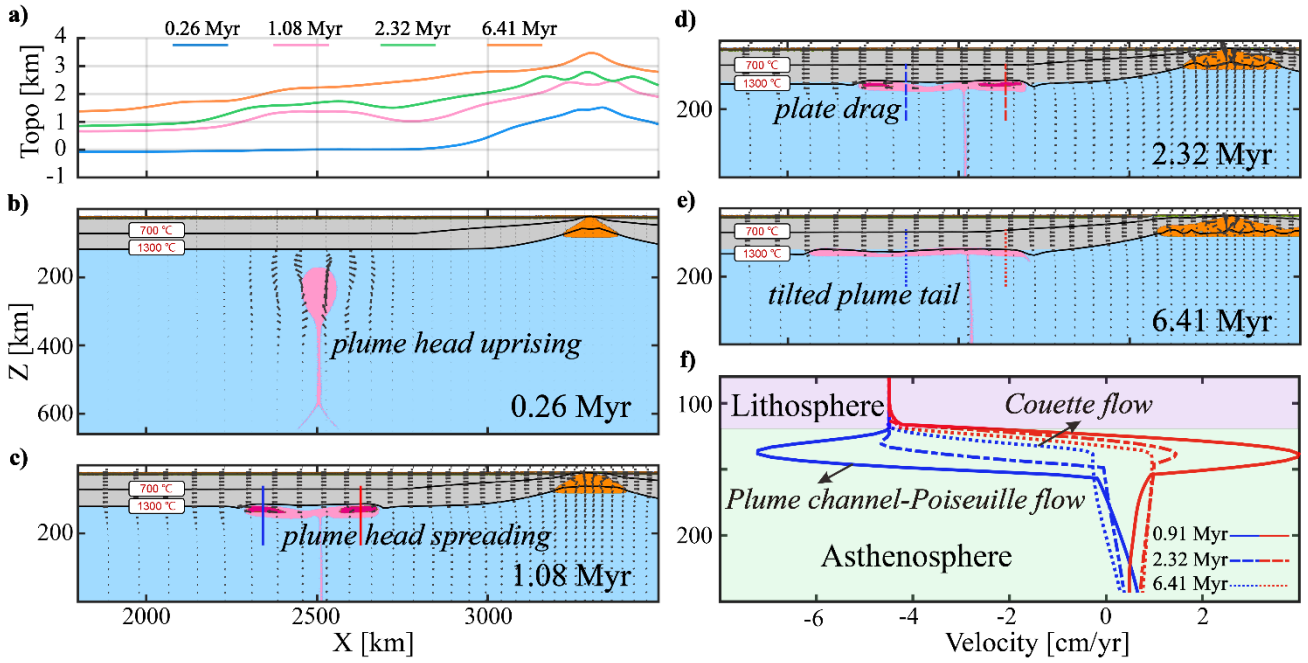

Figure 4. Same as Figure 3 for case M77 (i.e., the reference model for the plate-drag plume flow regime). The main model parameters employed in this case are: half spreading rate of 45 mm yr^{-1}, an initial plume head radius of 100 km, and an off-axis distance of 800 km.

The underlying mechanism ~~of~~for dominant plate-drag plume flow is the ~~shearing~~frictional shear force of the ~~spreading~~moving plate, which is further demonstrated by the plume flow velocity profiles (Fig. 4f). In the early plume head stage (~~0.91~~1.08 Myr), the plume spreads ~~away from the MOR~~out faster than ~~the~~ plate velocity~~; accordingly, plate drag actually inhibits the plume spreading~~, which is primarily driven by the overpressure of the ponding plume head at this stage. After a ~~certain~~short amount of time (~2.32 Myr), however, plume spreading becomes significantly slower than plate velocity, and hence plate- drag drives and controls ~~passive~~the plume flow. ~~Flow~~ Indeed, the flow mode

in the asthenosphere rapidly shifts from Poiseuille flow (i.e., active plume flow) ~~shifts progressively~~ to Couette flow (i.e., passive plume flow) (Fig. 4f), indicating the increasing role of plate drag on plume flow~~.~~, soon after an initial of plume-head spreading.

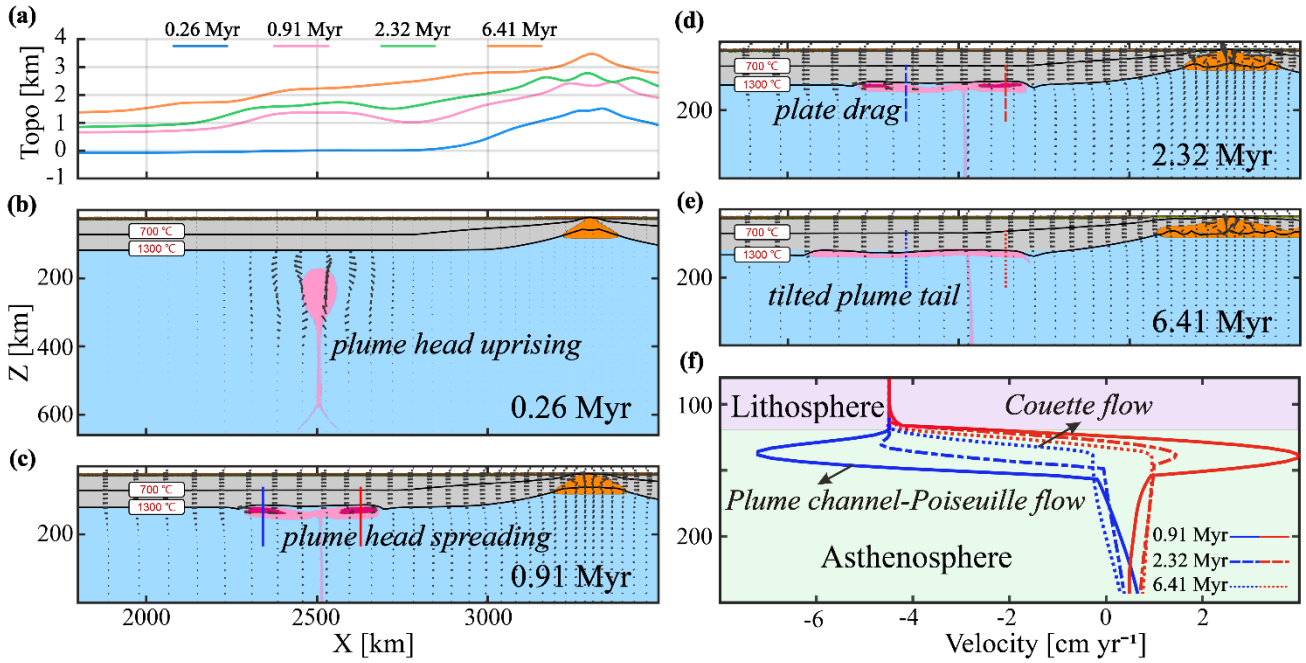

~~**Figure 4.** Reference model evolutions of plate-drag on plume flow. The major model parameters employed in this case are: the half spreading rate of 45 mm yr^{-1}, the plume radius of 100 km, and the off-axis distance of 800 km. **(a)** topography evolutions along the flow path of selected snapshots. **(b-c)** snapshots of reference plate-drag dominated model in compositional domain. Solid, dash and dotted lines are the velocity profiles of plume branches 100 km aside the plume stem and plot in f. **(f)** mantle flow velocity structure evolutions of ridge-ward and dragged plume domains marked in red and blue lines, respectively.~~

~~Weakening of the overlying oceanic lithosphere and melt extracting have been observed to occur in these set of models (Figs. 5e, f). The motion between rigid plate and viscous plume material alters the lithosphere stress similarly. However, thick and cold lithosphere prevents magma from venting.~~

Only a small fraction of molten plume is extracted to the surface when plume is dragged away. As the plume continues to cool, plume activity decay and partially molten plume gets solidified speedily. As a result, the heat flux at the surface is much lower (Fig. 5f).

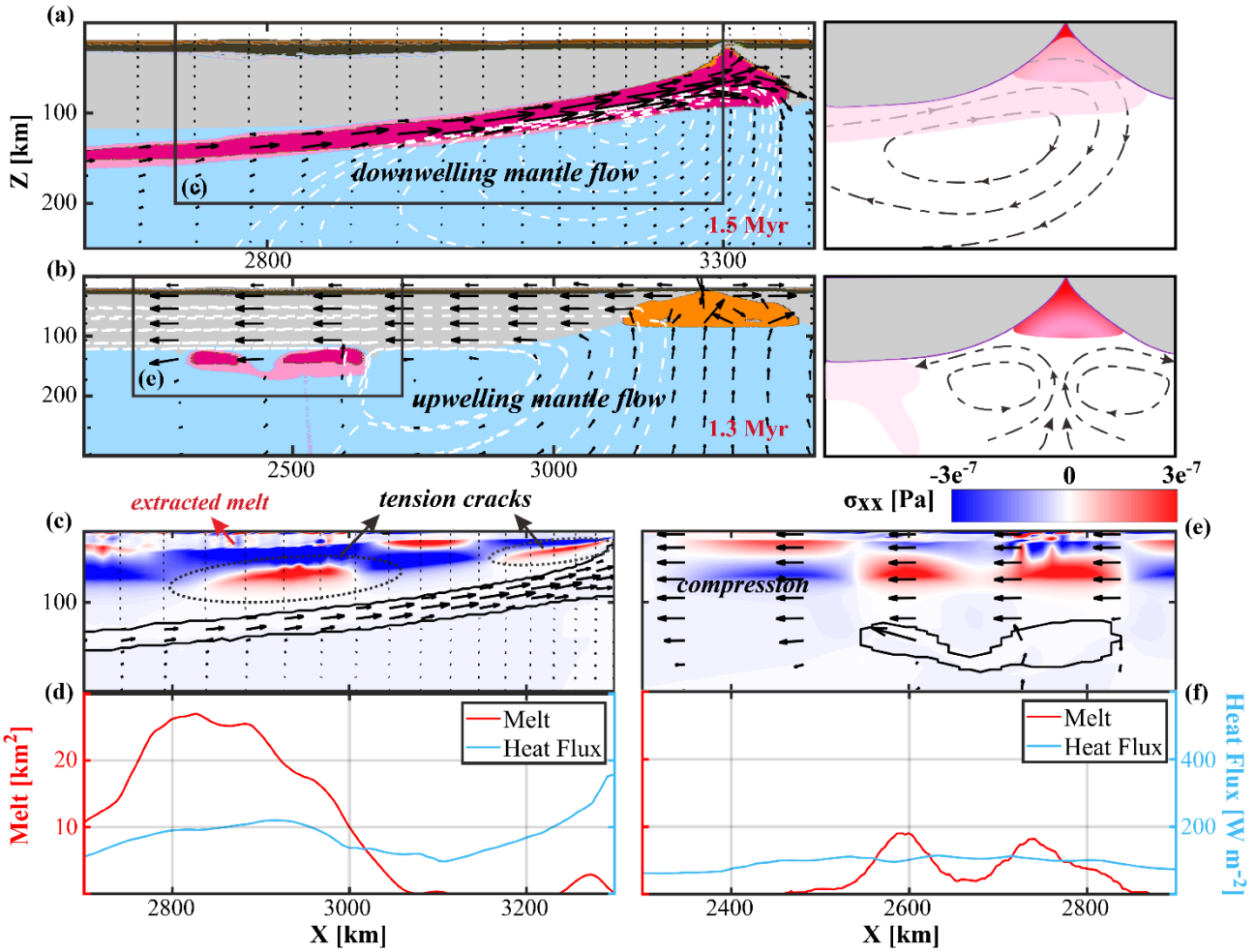

Figure 5. Comparsion between model evolution leading to ridge suction and plate drag mode on mantle plume. **(a)** Ridge sucks mantle plume with downwelling mantle flow (reference suction dominated model results: Fig.3). **(b)** Plate drags plume away with upwelling mantle corner flow (reference plate drag dominated model results: Fig.4). White dash lines are the streamlines. Schematic cartoons of ridge suction and plate drag pattern plot in the right panels. **(c, e)** Normal stress along lithosphere of black selected area in (a), (b). **(d, f)** Volume of extracted basalts and heat flux in overhead

~~lithosphere. Red lines show the extracted basalt volume within oceanic crust, and blue lines refer to the surface heat flux. Bulk of melt extract on the surface through the tensile cracks.~~

~~3.3 ridge suction versus plate drag~~

~~The ridge suction and plate drag~~

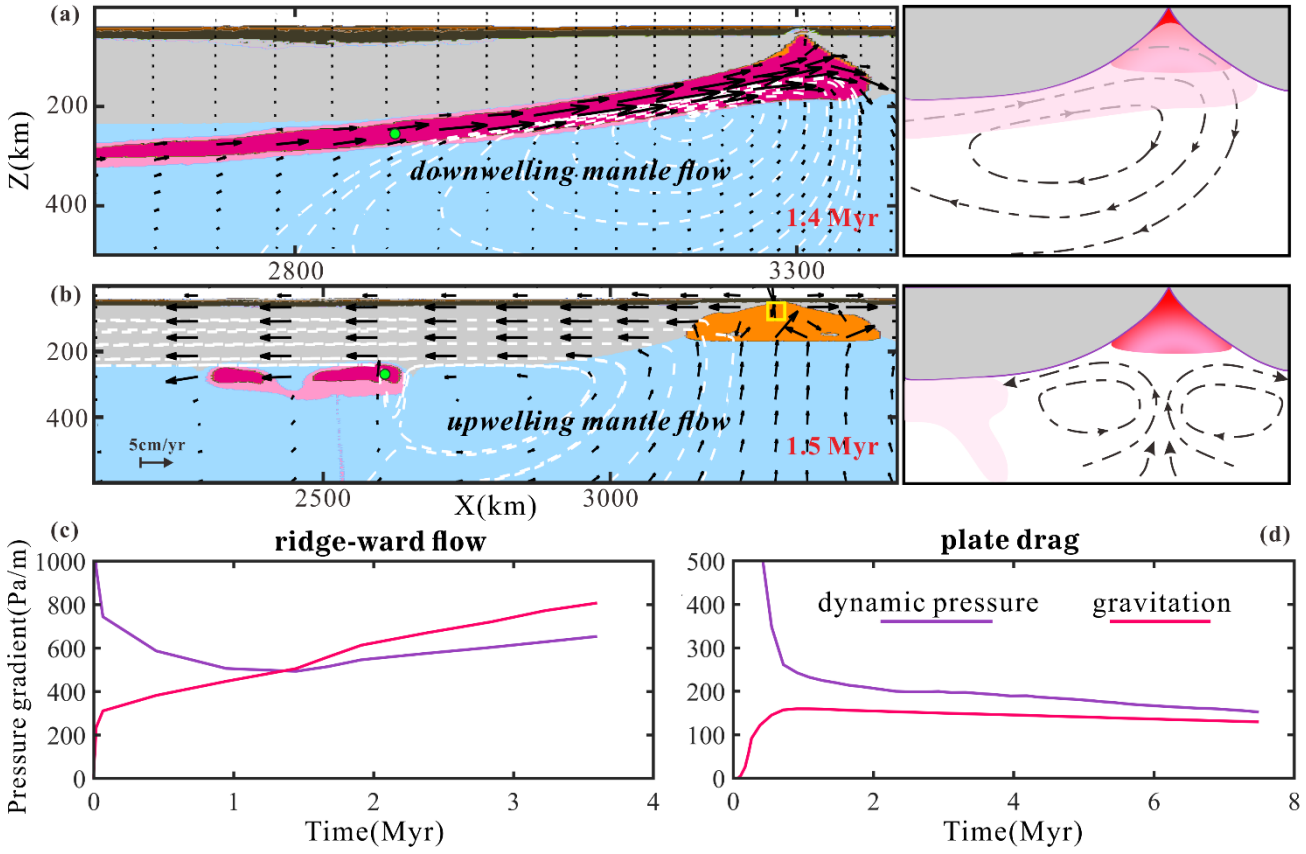

Figure 5. Comparsion between models with ridge-ward vs. plate-drag plume flow. **(a)** Ridge-ward flow with downwelling beneath the MOR (results from case M12 as in Figure 3). White dashed lines are streamlines; black arrows visualize the flow field. Schematic of flow in the sub-panel on the right-hand side. **(b)** Plate-drag flow with upwelling mantle corner flow beneath the MOR (results from case M77 as in Figure 4). **(c)** The dynamic pressure and gravitational gradient of plume marker (i.e. green circle in (a)) over time. The yellow box in (b) marks the location for the computation of average dynamic pressure at the ridge, needed for the calculation of the dynamic pressure gradient (see text).

(d) The dynamic pressure and gravitational gradient of plume marker (i.e. green circle in (b)) over time.

3.3 Two modes of plume-lithosphere interaction

The dominant ridge-ward and dominant plate-drag plume flow regimes are two distinct modes of plume-~~ridge~~plate interaction. The differences between these two ~~types of modes~~regimes are further demonstrated in terms of mantle flow (~~Fig. 5) and parameter effects~~Figs. 5a,b), driving forces (Figs. 5c,d). ~~6,7).~~

In the ridge~~-suction~~-ward dominated models, clockwise mantle ~~flow could form~~develops from the plume to the spreading ridge (Fig. 5a). A large amount of molten plume material flows to the spreading ridge and occupies the space underneath the ridge axis~~.~~, sustaining significant asymmetry of mid-ocean ridge melting (Conder et al., 2002). As a consequence to the continuous supply of the plume material, downward mantle flow forms beneath the ridge axis. This flow pattern dramatically differs from that shown in the plate~~-~~-drag dominated models, which show upward mantle flow underneath the ridge axis (Fig. ~~5b). Mantle corner flows are generated in~~5b), as typical for the ~~plate-drag dominated models, which block~~flow beneath a MOR without the influence of a plume~~-flow towards the ridge. Such mantle flow blows down the plume tail, and the moving plate carries away the subsequently upwelling plume material. These two distinct modes of plume-ridge interaction (ridge suction vs. plate drag) are controlled by model parameters (Fig. 6).~~.

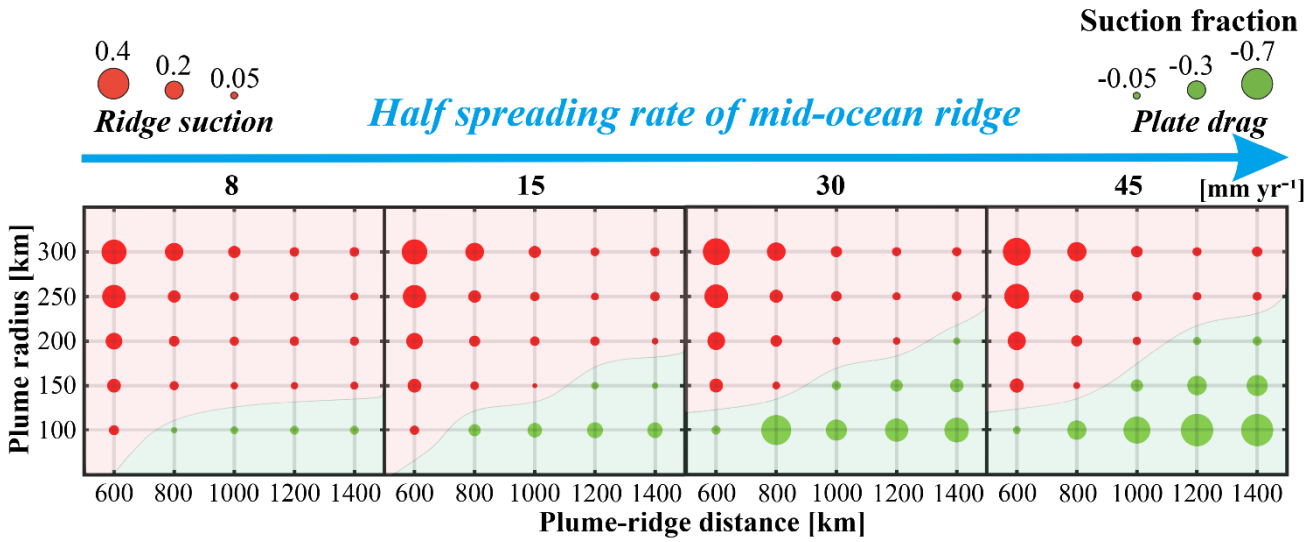

Figure 6. Parameter regime of the contrasting plume-ridge interaction modes. Suction fractions (the ratio of net volume difference between plume material transports ridge-ward and excludes away from ridge, Eq.(10)) at ca.8 Myr after plume head expansion. Each of the circles represents one of the numerical experiments, and sizes refer to the suction fractions. Circles in green represent ridge dragging away the plumes, whereas red circles display plumes are sucked to the ridge axis dominantly.

The distinct modes of plume-ridge interaction (ridge-ward vs. plate-drag flow) are controlled by the competition of the tectonic (plate drag, ridge suction) and gravitational (plume buoyancy) driving forces. On one hand, The moving plate drags sub-lithospheric plume material away from the ridge. On the other hand, the mechanism of ridge-ward flow is twofold. First, the buoyant plume material flows along the sloping base of the lithosphere towards the shallow ridge along the gravitational gradient. Second, the plume is driven along the dynamic-pressure gradient from the pressure maximum (e.g., where the plume sustains dynamic topograph) towards the pressure minumum beneath the diverging ridge. These gravitational (G_{gv}) and pressure-driven (G_{dp}) gradients are calculated by tracing plume markers (Figs. 5c,d) as follows:

$$G_{dp} = (P_{mk} - P_r)/L \quad (12)$$

$$G_{gv} = (\rho_0 - \rho_{mk}) * g * k \quad (13)$$

where P_{mk} is the dynamic pressure of plume marker and P_r is the averaged pressure in a 50 km box at ridge center (Fig. 5b); L is the horizontal distance from plume marker to ridge axis; ρ_{mk} and ρ_0 are the plume marker density and initial density, respectively; g is the gravitational acceleration; k is the local slope of the base of the lithosphere.

In the early stage of model evolution, the plume head's dynamic overpressure is dominant, driving plume spreading in both directions (Fig. 5c), in particular in the direction of the low-pressure ridge. However, this pressure gradient systematically diminishes over time as the plume (head) spreads. Once the spreading plume approaches the ridge, the lithospheric slope increases. At some point, the gravitational gradient exceeds the dynamic pressure gradient, taking over as the major driving force of guiding plume material towards the ridge. Consequently, one of the essential conditions for plume-ridge interaction is that the plume must be able to reach the critical zone near the ridge, where the slope is sufficiently steep to take over for the ever diminishing pressure gradient. This implies that the plume buoyancy must (1) overcome the shearing force of plate drag, and (2) the pressure-gradient must be sustained long enough to reach the critical zone, in which the gravitational gradient can take over. The (1) shearing force scales with the rate of ridge spreading, and the (2) critical zone is more readily reached for high buoyancy fluxes at a given plume-ridge distance.

3.4 Influence of model parameters

We have systematically investigated the effect of the three main model parameters (i.e., the

spreading rate of the mid-ocean ridge, initial plume head radius and ~~initial off-axis~~plume-ridge distance ~~of plume~~) on plume-ridge interaction ~~(Fig. 6).~~. We explored half spreading rates of the ~~mid-ocean~~ ridge of 8, 15, 30, and 45 mm yr^{-1}, corresponding to ultra-slow, slow, medium, and fast-spreading mid-ocean ridges, respectively (Gerya, 2012). We varied initial plume head radii in the range of 100 km to 300 km. Further, ~~the~~we tested ~~off-axis~~plume-ridge distance ~~ranges from~~in the range of 600 to 1400 km.

~~Generally, the~~**3.4.1 Plume head radius**

The size of the buoyant plume exerts ~~a major~~an important control on plume-ridge interaction. Small plumes tend to be dragged away from the ridge, with typically larger lateral fluxes of the left branch than the right branch of the spreading plume (Figs. 6a,b). The buoyancy flux in each branch is calculated by multiplying the velocity of the markers in~~7a-c). As~~ plume pipe (Figs. 6d-f) by the density. The dynamic ~~overpressures are~~pressure decreases with decreasing plume size (Fig. S8a), and the pressures gradient is thus not strong enough for small~~, plate~~ plumes to reach the ridge. Plate shearing dominates ~~mantle~~plume flow soon after plume head spreading~~. The~~, and the moving plate then drags plume head material, ~~and leaves~~leaving a tilted plume tail (Fig. ~~7d~~6d). In contrast, ~~plumes~~ with larger ~~radii~~initial plume head radius or buoyancy ~~fluxes~~flux, the ponding plume spreads more vigorously (Fig. 6c) and sustains much higher overpressures at the base of the plate~~.~~ (Fig. S8a). This vigorous spreading can overcome plate drag to drive Poiseuille flow in both directions ~~(Fig. 7c).~~. Once the right plume branch approaches the spreading center, it is attracted and further accelerated by ridge suction. The plume tail is also markedly tilted towards the ridge axis due to asymmetric spreading ~~in the dynamic pressure field of the MOR.~~(Fig. 6f). The larger the plume is, the more plume material gets entrained by the spreading center.

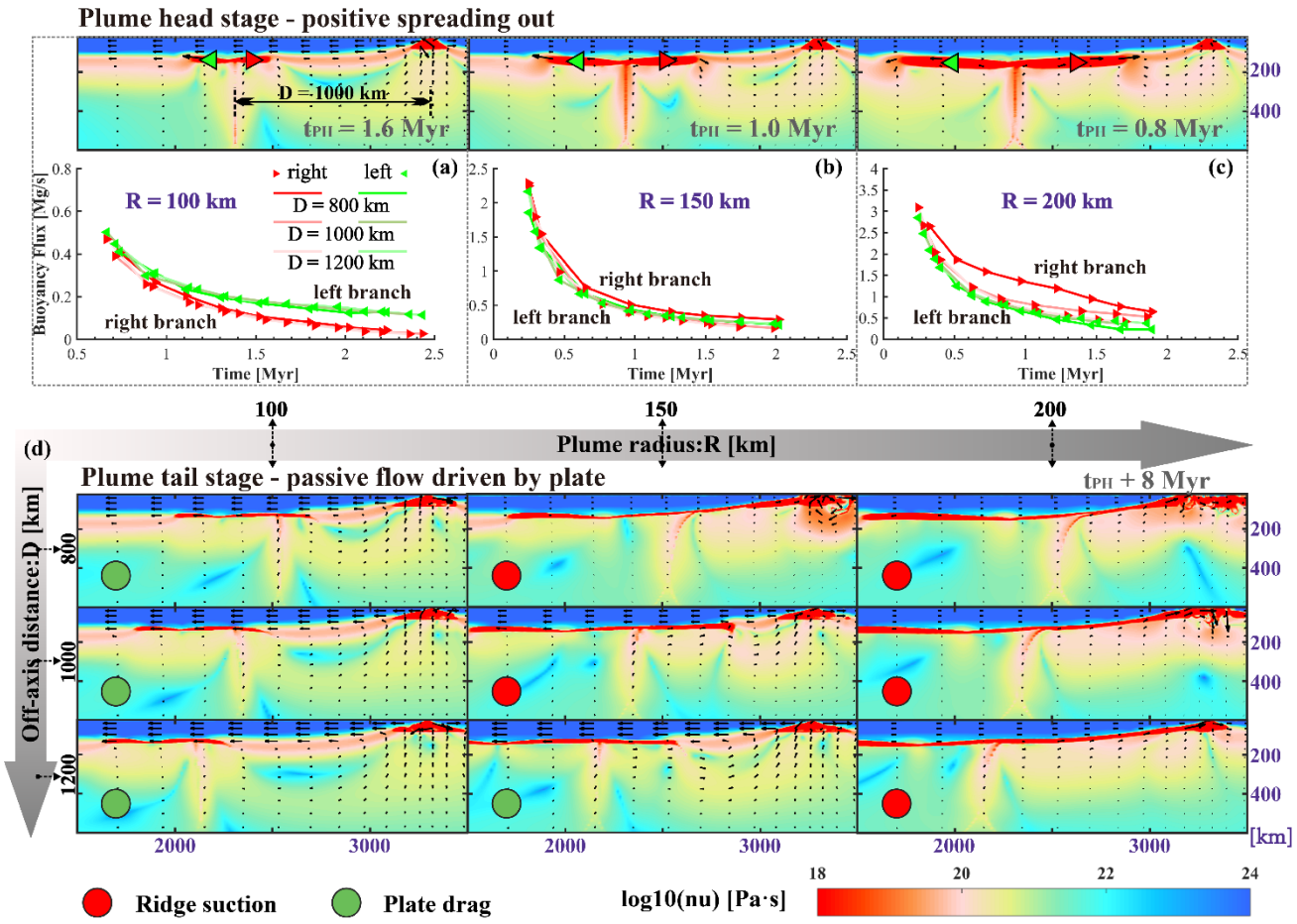

~~Figure 7.~~ ~~Parameter regime showing ridge suction versus plate drag in the selected parameter space.~~ ~~(a-c) Time evolution of~~

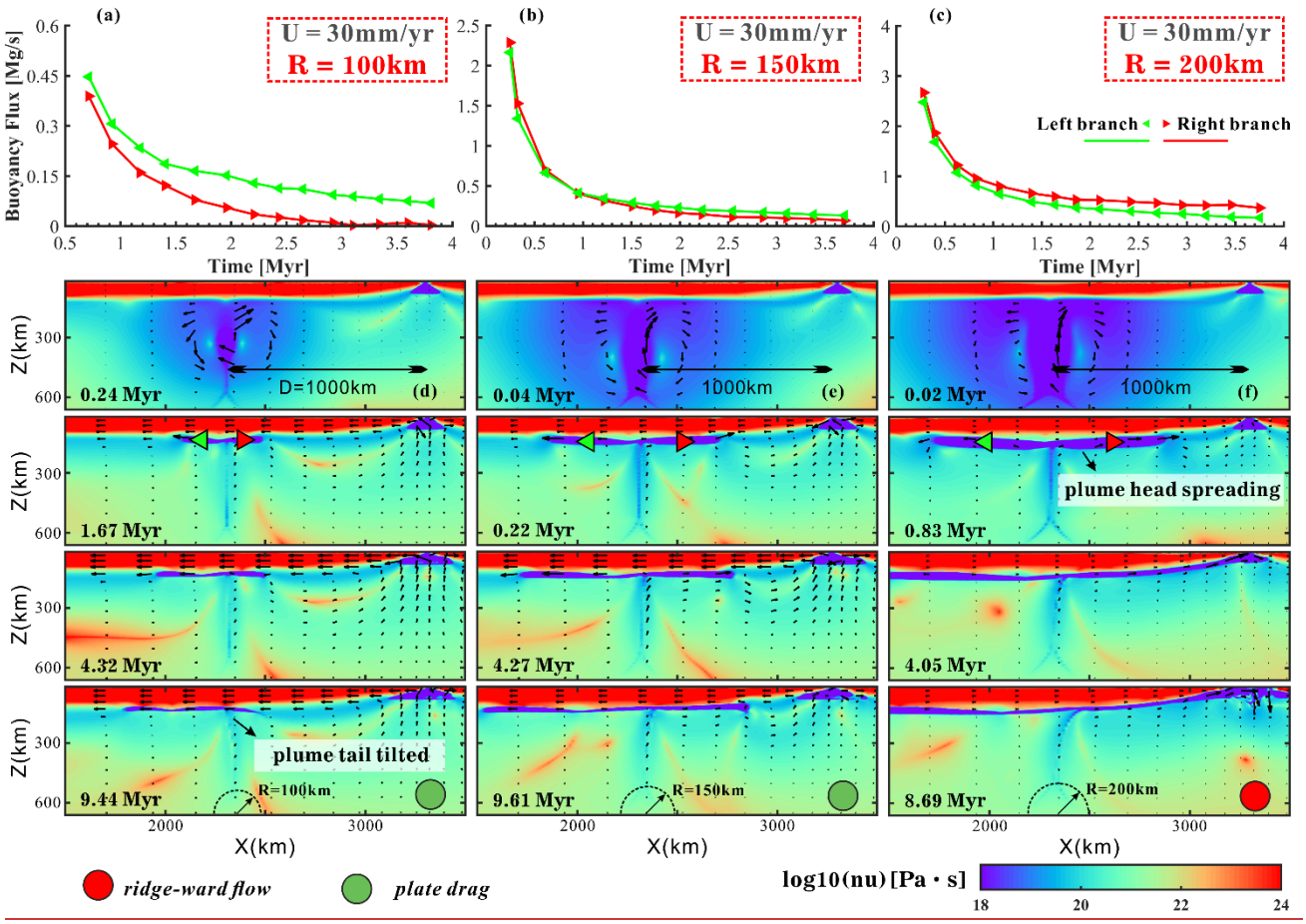

Figure 6 Models varying initial plume head radii (model M53, M58, and M63, Table S1 in supplementary material) shown by buoyancy flux and viscosity. **(a-c)** Buoyancy flux in spreading plume branches ~~with varied plume size and off-axis distance at plume head stage.~~over time. Green and red triangles are ~~tracers~~markers used for buoyancy flux calculation. **(d-f)** Viscosity snapshots of models with different plume ~~size, plume-ridge distance at ca.8 Myr after plume head ponding (t_{PH}) beneath the plate are shown.~~head radii. Models with green circle represent plate ~~-~~drag ~~dominated pattern~~plume flow and ridge ~~suction~~ -ward plume flow in red.

~~Moreover, plume~~**3.4.2 Plume-ridge distance**

Plume-ridge distance also controls the regime of plume-ridge interaction. A plume at large distances spreads similarly ~~with~~as a plume at a small distance, but is less likely to get affected by ridge suction (Figs. ~~7b,d~~7e,f). The ~~dynamic~~ pressure gradient ~~is exactly what drives the flow~~ between the plume and ridge~~. The~~ drives the ridge-ward plume flow. However, the larger the plume-ridge distance, the smaller the pressure ~~gredient~~gradient would be (Fig. S8b), resulting in a lower buoyancy flux across the plume pipe (Figs. 7a-c). ~~.~~In the cases of distant plumes, the spreading of the plume head is strongly affected by plate drag (Figs. 7b, c). On the other hand, the difficulty in ~~creating plume-~~sustaining ridge ~~connection in the case~~-ward plume flow may also link to the heat transfer between the cold plate and the hot plume rocks. With gradually cooling from upper plate by heat conduction and diffusion, the viscosity of plume increases ~~with the reduction of temperature.~~as it cools. Such increasing viscosity slows the plume down, ~~inhibiting the flow to ridge consequently (Fig. 7d). Previous studies indicated that the extra travelling time needed for an additional 200 km of plume to reach~~stopping the ridge ~~is roughly equal to the thermal diffusion time for a 20 km thick, sub-horizontal~~-ward plume ~~channel cooled from above rigid lithosphere (Kincaid et al., 1996).~~flow eventually (Figs. 7e, f). Hence, for ~~those distant cases, it takes longer time for~~ cases with large plume-ridge distances and hence travel times, the ponding plume ~~material to reach the ridge, during which the ponding plume head is exhausted~~head cools and is ultimately carried away by the moving plate.

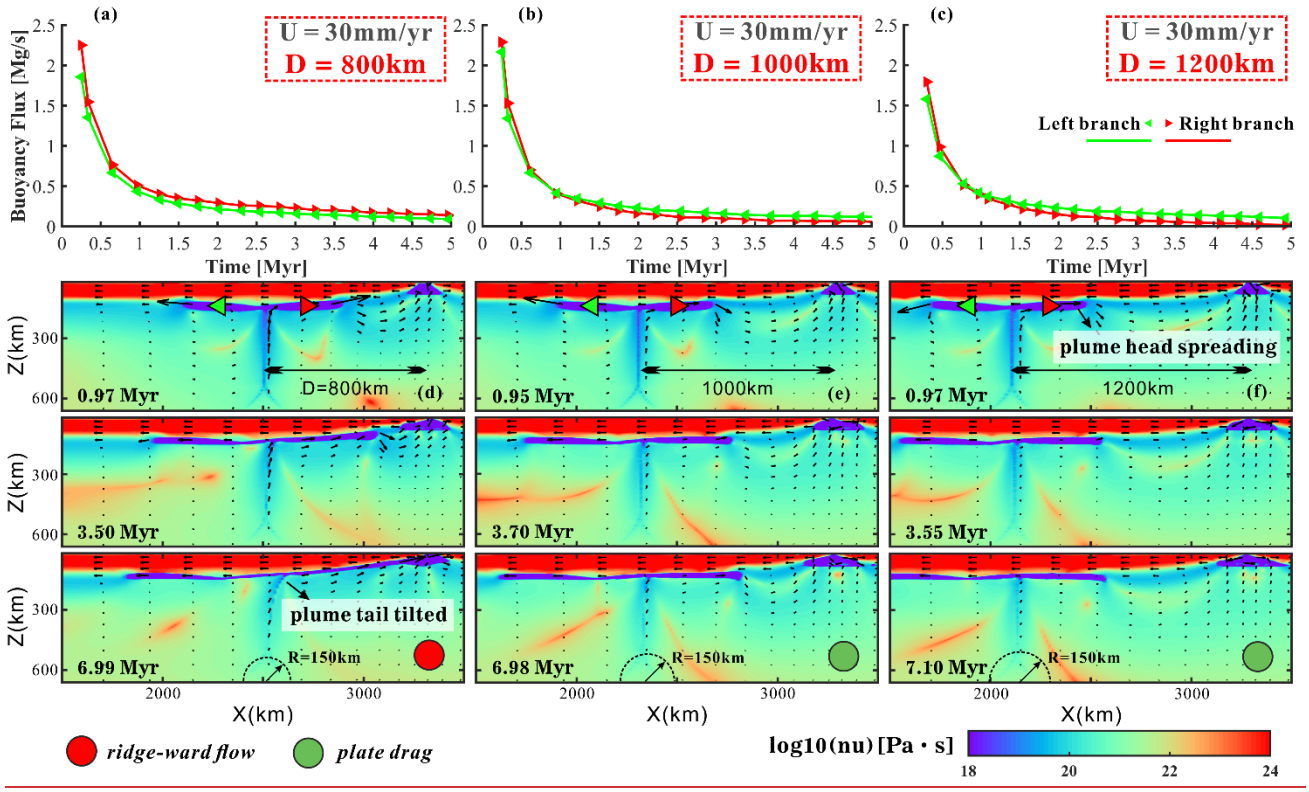

Figure 7. Models varying plume-ridge distances (model M57-M59, Table S1 in supplementary material) shown by buoyancy flux and viscosity. **(a-c)** Buoyancy flux in spreading plume branches over time. Green and red triangles are markers used for buoyancy flux calculation. **(d-f)** Viscosity snapshots of models with different plume-ridge distances. Models with green circle represent plate-drag plume flow and ridge-ward plume flow in red.

3.4.3 Half spreading rate of ridge

Another parameter that is worth investigating is the spreading rate of the ridge. The modeling results indicate that fast-spreading ridges promote plume flow away from the ridge due to the friction (Figs.8 and 9a). With increasing spreading rate, the effect of plate shearing on plume-lithosphere interaction increases, as quantified by the ~~suction~~spreading fraction. The ~~suction~~spreading fraction γ (Eq.(~~10~~14)) is defined here as the ratio of ridge-ward vs. plate-drag plume volume fluxes ~~transported ridgeward and dragged away from the ridge, and a proxy to evaluate the relative strengths of ridge~~

~~suction and plate drag.~~. We integrated the ~~sucked~~ridge-ward plume volume flux (right branch), ~~V_{sp}~~V_{rw}, and ~~dragged~~plate-drag plume volume flux (left branch), ~~V_{ep}~~V_{tw}. V_p is the total plume volume flux in the model. Ridge~~-suction~~-ward plume spreading is dominant for positive γ; plate~~--~~drag plume spreading is dominant for negative γ.

$$\gamma = ~~(~~V_{sp}(V_{rw} - ~~V_{ep}~~V_{tw})/V_p \qquad (~~10~~14)$$

In the early stage (~1 Myr), pressure-driven flow dominates in all models and spreading fractions are positive, mainly driven by the expansion of the overpressured plume heads along the pressure gradient. After a certain time, the spreading fractions decrease dramatically with the decay of the mantle plume activity, representing the transition from the ridge-ward to the plate-drag regime in some cases. The characteristic ~~suction~~spreading fractions after 8 Myr model time as a function of our model parameters are shown in Fig. ~~6~~8. This compilation of our results ~~indicate~~reveals that the dominance of ridge~~-suction~~-ward flow decreases with increasing spreading rate and off-axis distance, but significantly increases with plume size~~-significantly.~~. For models with fast-spreading ridges, the parameter range of plate~~--~~drag flow dominated models is expanded, indicating ~~that plumes flow away from~~ the ~~mid-ocean ridges is promoted by higher plate velocities.~~

~~4 Discussion~~

~~4.1 Effects~~critical role of ~~spreading rate on~~ plate drag

~~The spreading rate of the mid-ocean~~ in restricting ridge ~~affects~~-ward flow and plume-ridge interaction~~, and the modeling results show that fast-spreading ridges promote dragging of plumes due to plate friction (Figs. 6, 8a). Here, we further demonstrate the effect of spreading rate on plume motion. Firstly, the calculation of suction fractions γ (Eq.(10)) over time shows the switch from dominant ridge suction to dominant plate drag (Fig. 8b). In the early stage (ca.1 Myr), ridge suction plays the dominant role in all these models, mainly due to the active expansion of the plume heads to the low pressure centers underneath the spreading ridges. After a certain time, the suction factors decrease dramatically with the decay of the mantle plume activity, representing the transition from ridge suction to plate drag dominated stage~~.

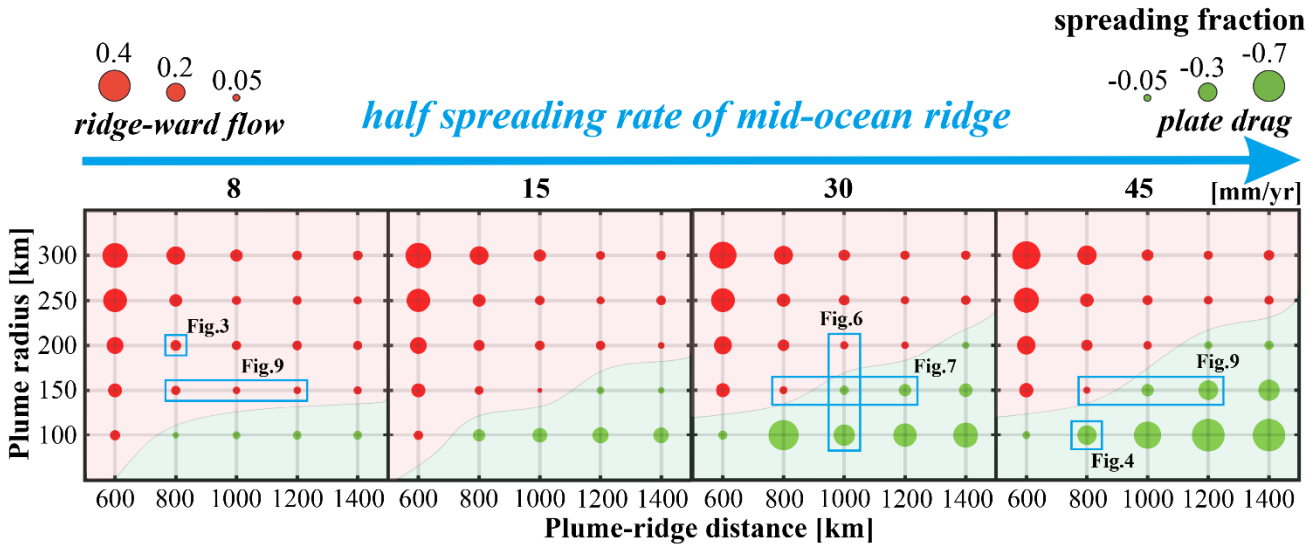

Figure 8. Parameter regime diagram of the contrasting modes of plume-ridge interaction. Spreading fractions γ (Eq. (14)) at ~8 Myr model time. Each of the circles represents one of the numerical experiments, and sizes refer to γ. Circles in red and green represent models with dominant ridge-ward plume flow and plate drag, respectively.

The transition from ridge ~~suction~~-ward (positive γ) to plate ~~-~~-drag (negative γ) flow in some of our cases is mainly determined by the competition between the effects of pressure-driven plume head spreading ~~(overpressure in the plume head stage)~~ and plate shearing. The overpressure in the plume head drives plume materials ~~to~~towards the lower pressure spreading center, while the moving plate shears plume away. Hence, we quantify the shear force of the overriding oceanic plate on the plume head using an integral approach ~~and the pressure diffenence between plume head and ridge center.~~:

$$F_s = \int \sigma_{xz}\, dA \quad (\text{~~11~~}15)$$

Equation (~~11~~15) is employed to calculate the shear force, where F_s is the total shear force the spreading oceanic plate exerts on the uppermost part of the plume. σ_{xz} is the shear stress on each mantle plume gird cell, A refers to the area of each grid cell. The pressure ~~difference is~~gradients, both gravitational and dynamic pressure, are calculated ~~from~~by tracing the ~~averaged pressure in a 50 km box of~~plume markers according to equations (12-13). As the plume ~~head and ridge center (Fig. 8a). As plume~~ material rises to the base of the lithosphere ~~base~~, the shear force ~~from~~exerted by the plate increases over time. We find that the integrated shear force between the spreading plate and the plume increases significantly as half spreading rate increases (Fig. ~~8c), indicating larger plate friction force that the fast-spreading plate exerting on the plume head.~~9c).

~~Conversely, the spreading of the ridge contributes to the pressure-driven suction of plume materials. During the plume head stage, dynamic pressure of plume rises, and the ridge suction is able to overcome the plate drag, pumping plume to the ridge. However, without plume further supplies, the overpressure difference from the plume head to the spreading center decreases slowly with time (Fig.~~

~~8d). The plume branches get cool and their vitality is greatly reduced. As soon as plume push decreases, the suction fraction turns negative (Fig. 8b). More importantly, increasing the spreading rate of ridge generates a smaller overpressure difference. The faster the ridge spreads, the lower the dynamic pressure gradient driving the ridge suction. Thus, strong plate shearing force, combined with small overpressure difference, will significantly suppress the plume-ridge interaction and gradually drag the buoyant plume material away from the ridge. In addition, while all models gradually switch from ridge suction in the plume-head stage to dominant plate drag in the plume-tail stage, the model with fast-spreading rate shifts much sooner than that with slow-spreading rate.~~

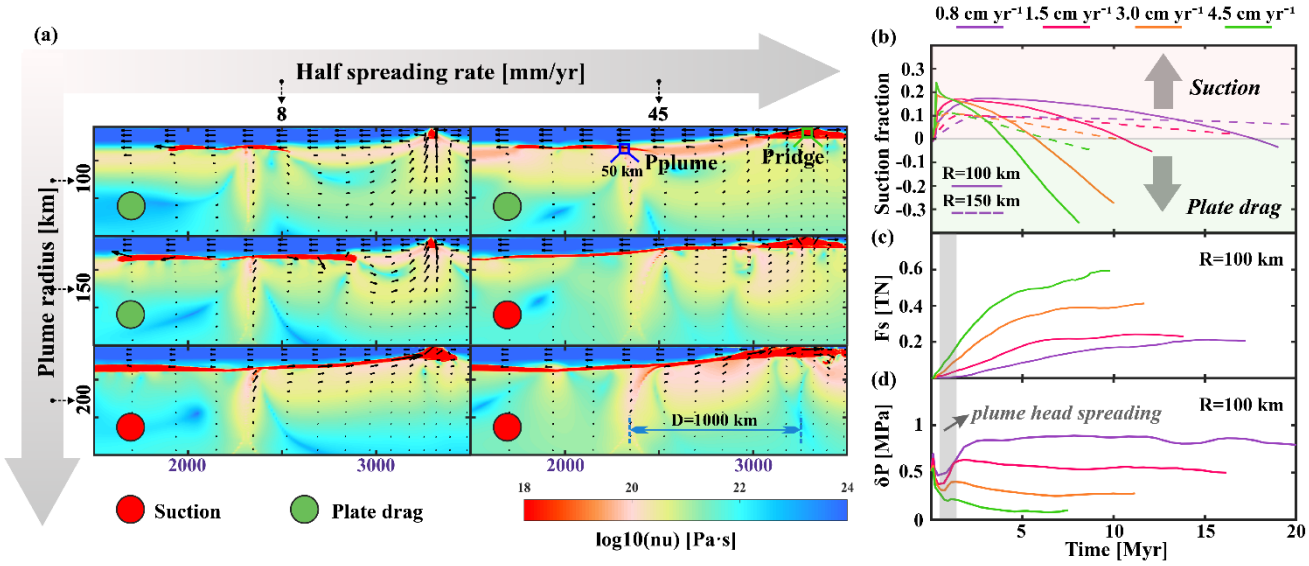

Conversely, ridge spreading rates control gravitational and pressure-driven plume driving forces (Fig. 9d). Increasing the spreading rate of the ridge implies a smaller dynamic pressure gradient, because the pressure gradient is related to the plate thickness difference at the ridge and plume, which is dependent on the spreading rate. A fast-spreading ridge also implies a smaller gravitational gradient, because it leaves a more shallowly-dipping lithospheric base. Thus, relatively strong plate shearing combined with relatively small pressure and gravitational gradients tend to advance plate-drag plume flow for high spreading rates.

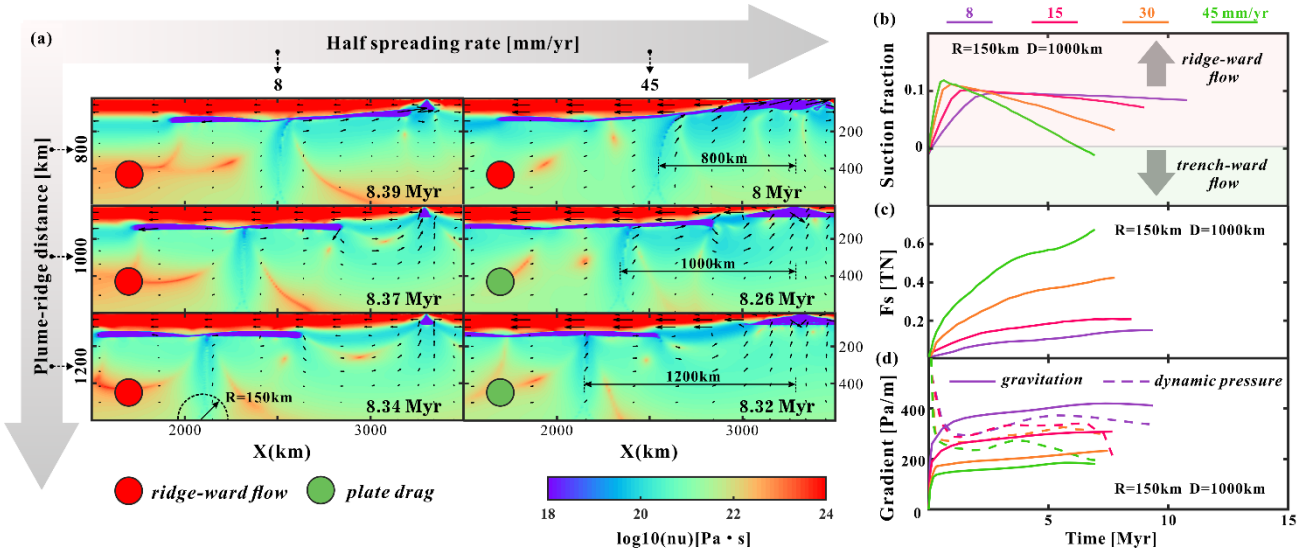

Figure ~~8~~9. Model results influenced by different half spreading rates. **(a)** Effect of spreading rate on ridge ~~suction verse~~-ward flow vs. plate--drag~~. viscosity~~ flow. Viscosity snapshots are shown~~.~~ (model M7-M9, M82-M84, Table S1 in supplementary material). Fast-spreading ridge ~~promote plume dragging.~~promotes plume material dragged. Models with green circle represent plate-drag plume flow and ridge-ward plume flow in red. **(b)** Dynamic evolutions of ridge ~~suction~~-ward and plate--drag ~~on~~ plume flow, revealed by defined ridge ~~suction fraction (the ratio of net volume difference between plume material transports ridge-ward and excluded away from ridge).~~spreading fraction (eq.14). **(c)** Shear force (*Fs*) between moving plate and plume material under different spreading rates. ~~**(d)** Overpressure difference (δP: Pplume – Pridge)~~**(d)** Pressure gradient between plume head and ridge center ~~of~~in different half spreading ~~rates~~rate models. The ~~overpressure in ridge~~solid and ~~plume~~dash lines are the ~~mean~~plume gravitation and dynamic pressure ~~of 50 × 50 km box in (a).~~gradient, respectively.

4 Discussion

Natural observations show that there are only very few hotspots indicative of ridge-ward plume flow close to the East Pacific Rise (EPR) (Fig. 10a), in contrast to many such hotspots in the Atlantic and Indian oceans. A previous study (Jellinek et al., 2003) proposed that fast-spreading ridges ~~**4.2 Plate drag dominated at**~~ such as the ~~**East Pacific rise?**~~

~~The tested plume size, plume-ridge distance and spreading rates of mid-ocean ridges largely affect the plume-ridge interaction. Natural observations show that, unlike the wide distributed of plume-ridge interactions along the Atlantic and the southwest Indian mid-ocean ridges, there is not much hotspots close to the east Pacific rise (Fig. 9a). A previous study (Jellinek et al., 2003) proposed that fast-spreading ridges exert strong ridge suction on plumes and attract the~~EPR efficiently convey any surrounding plumes ~~entirely to~~into the spreading ~~centers~~center from the deep mantle (Fig. 1c), which leads to fewer hotspots ~~along the~~ nearby fast-spreading ridges. However, based on our modeling results, ~~we propose that~~ fast-spreading ridges ~~are more likely~~tend to ~~push away plumes~~promote plate-drag flow of the spreading plume material, providing an alternative explanation to the relatively absence of hotspots along the ~~East Pacific Rise.~~EPR. We discuss the ~~possibility~~viability of this ~~assumption combined~~potential explanation by comparing with geological and geophysical observations (Fig. ~~9~~10).

Firstly, the plate drag effect of fast-spreading ridges on plumes is evidenced by geophysical observations. ~~We locate the positions of the mantle plumes at the core-mantle boundary (CMB) and the associated hot spots on the surface based on the recent study (Jackson et al., 2021). The offset between the deep and surface position of plumes is a common feature, indicating the tilt of plumes due to mantle flow. Specifically, a large portion of plumes located in the Atlantic Ocean tilt to the mid-ocean ridges. However, very few plumes in the Pacific Ocean tilt to the mid-ocean ridges, and the majority of plumes move away from the ridges, indicating the significant effect of dragging by the~~

~~fast spreading ridges. These indications imply that the plumes are more likely to bend by shallow mantle flows, such as backflow due to plate subduction or ridge spreading. Such observations are consistent with the predictions of plate drag model which well explains the absence of hotspots along the East Pacific rise~~We locate the positions of the mantle plumes at the core-mantle boundary (CMB) and the associated hot spots on the surface based on global seismic tomography (Jackson et al., 2021; Koppers et al., 2021). A lateral offset between the deep and surface positions of plumes is a common feature, indicating the deflection of plumes due to mantle flow. Specifically, a large portion of plumes located in the Atlantic are tilted towards the mid-ocean ridge. However, only very few plumes in the Pacific are tilted towards the mid-ocean ridge; indeed, the majority of plumes are tilted away from the ridges, indicating the significant effect of plate drag on plumes beneath fast plates. Such observations are consistent with the predictions of our models with dominant plate-drag plume spreading.

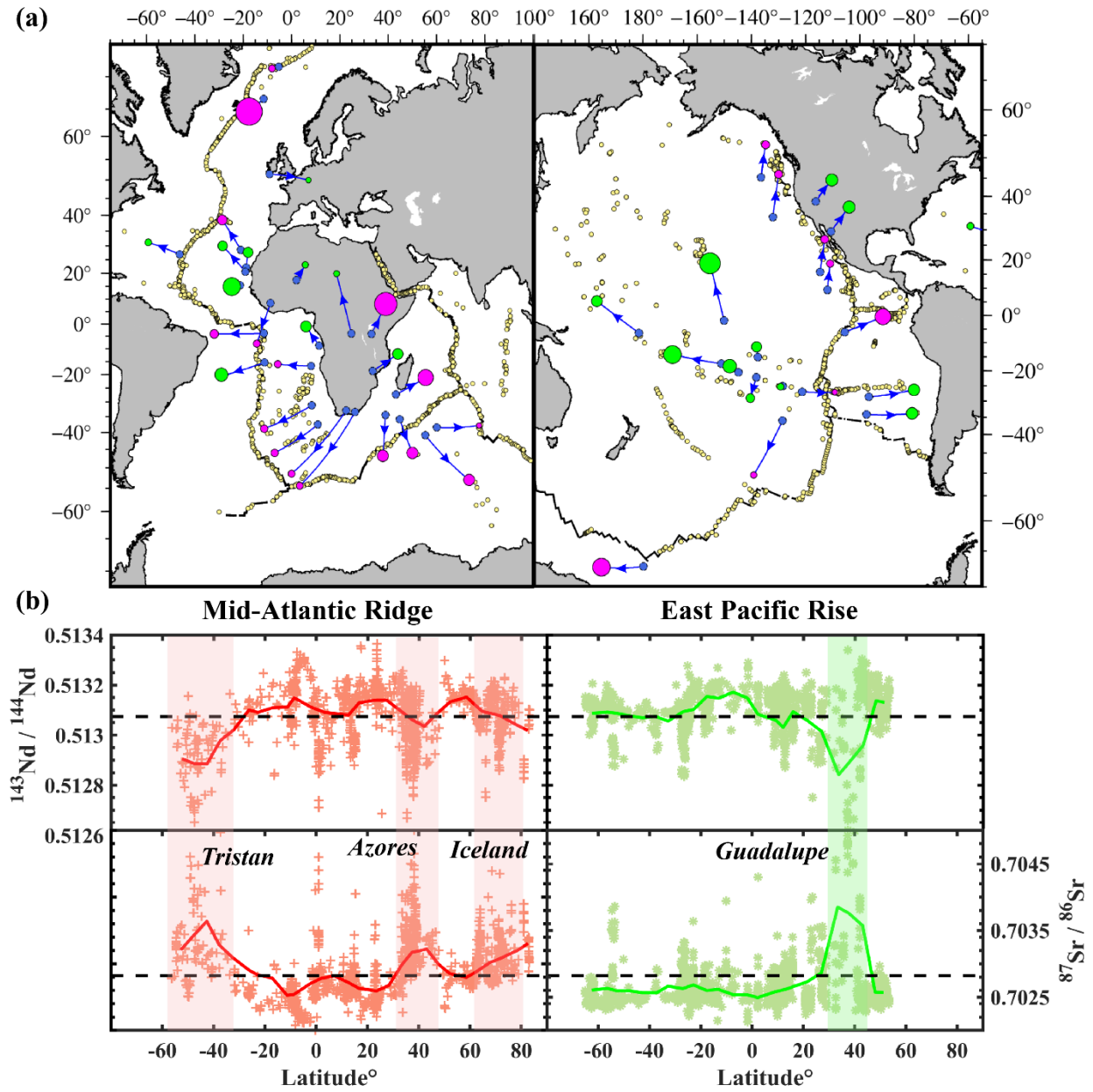

Figure 10. A compilation of hotspots along with spreading ridges in the Atlantic and the Pacific. **(a)** Distribution of surface hotspots (circles) together with depth-projected source locations at CMB (blue dots) of the plumes based on (Jackson et al., 2021). Plumes in magenta circles are mantle plumes interacted with ridges (Ito et al., 2003), and plumes not interacted with ridges are shown as green circles, whose size refers to the plume buoyancy flux (Hoggard et al., 2020). Yellow dots are MORB samples mapped in (b). **(b)** Plot of radioactive isotopes ratios along ridge MORB samples. The data are downloaded from the PetDB Database (http://portal.earthchem.org/). The colored symbols refer to

samples in different mid-ocean ridge. Main hotspots influencing MORBs are labeled with shaded bands. The black dash lines are the mean MORB isotopes ratio from ~~Geochemical studies suggest that mantle plumes, together with interacted MORs, are enriched in light rare earth elements (LREEs) and radiogenic isotopes of Sr and Pb but depleted in Nd isotopes. We find that both the Atlantic and east Pacific Oceans display heterogeneities along the ridge axis (Fig. 9b), indicating the mixture of plume material. However, the Mid-Atlantic ridge seems slightly more heterogeneous than the East Pacific rise in terms of geochemical isotopes. The East Pacific rise is basically characterized as normal oceanic basalt, along which only several regions show composition associated with nearby plumes.~~Gale (2013). Red and green lines are the mean ratios of the samples in Mid-Atlantic ridge and EPR, respectively.

Geochemical studies suggest that mantle plumes are enriched in light rare earth elements (LREEs) and radiogenic isotopes of Sr and Pb but depleted in Nd isotopes. These geochemical anomalies are evident in MORB at the sites of active plume-ridge interaction (Cushman et al., 2004; Douglass and Schilling, 1999; Yang et al. 2017). We find that MORB sampled along both the Mid-Atlantic ridge and the EPR indeed display geochemical anomalies (Fig. 10b), indicating ridge-ward flow of plume material at specific locations. However, the Mid-Atlantic MORB dataset is slightly more heterogeneous than the East Pacific Rise in terms of geochemical isotopes. The EPR is basically characterized as normal oceanic basalt, along which only very few regions show composition associated with nearby plumes. This contradicts the view (Jellinek et al., 2003) that mantle plumes are ~~incorporated~~fully entrained into the central ~~upwelling underneath the~~MOR melting zone at fast-spreading ridges.

Based on our modeling results, initial plume head radius and plume-ridge distance also control the

mode of plume-ridge interaction. However, there is ~~strongly influenced by plume radius, plume-ridge distance and velocity~~only a small difference in terms of the ~~plate. Most of~~fraction of interacting vs. non-interacting plumes ~~in~~ for different buoyancy fluxes B: a small majority of major plumes (5 of 8 with $B > 1.6$ Mg/s) vs. a small minority of small-to-intermediate plumes (11 of 25 for $B < 1.6$ Mg/s) display interaction with the ridge (Fig. 11a). The underlying cause for this observation remains unclear, but may be related to the distribution of large plumes globally with many of them being located very far from MORs. Also note that our 2D models are limited in that plume material cannot spread in the out-of-plane direction, hence somewhat exaggerating the effects of buoyancy flux. In any case, the distribution of observed plume buoyancy fluxes (Hoggard et al., 2020) varies little across different oceans (Fig. 11a). Therefore, the effects of plume size are not a good candidate to explain the notable difference between the Atlantic and Pacific ~~ocean, upwelling from the~~ in terms of plume-ridge interaction mode.

On the other hand, compared with the Atlantic and Indian Oceans, Pacific ~~super plume,~~plumes are located significantly further from the mid-ocean ridge (Fig. 11b). Plume-ridge distances in the Pacific are mostly >2000 km, which exceeds the maximum plume-ridge interaction distance of 1400 km (Schilling, 1991). Most plumes in the Pacific exhibit the typical signatures of plume flow away from the ~~MOR~~ridge, such as parabolic swell shapes (e.g., Society, Marquesas and Hawaii plumes; Ballmer et al., ~~2013~~2013a; Ballmer et al., 2015; Cheng et al., 2015; Wolfe et al., 2009), and linear volcanic chains ~~(Buff et al., 2021; Clouard and Bonneville, 2005; Jackson et al., 2010)~~(Buff et al., 2021; Clouard and Bonneville, 2005; Jackson et al., 2010). ~~These age~~Age-progressive hotspots trails indicate ~~the effects of plate drag on mantle plumes. However, it's noteworthy~~an absence of dominant ridge-ward flow. By contrast, most plumes in the Atlantic have been close to the ridge since the opening of the

ocean. These mantle plumes (e.g., Discovery, Iceland, Tristan-Gough; O'Connor et al., 2012) did not move much since the breakup of the Atlantic. One factor may be that the underlying plume generation zone (i.e., the edge of the African LLSVP) round largely parallel to the Mid-Atlantic Ridge (Fig. 1) (Torsvik et al., 2006). In this case, plume-ridge distance may play a critical role in the plume-ridge interaction, and could explain the striking difference between the Pacific and Atlantic in terms of the number of plume-ridge interacting vs. non-interacting systems. In addition, the rapid movement of the Pacific plate tends to inhibit ridge-ward plume flow at a given plume-ridge distance. The distribution of interacting (stars) vs non-interacting systems in Figure 11b is almost exactly as predicted by our models for the coupled effects of plume-ridge distance and plate velocity. For example, we note that fast-spreading ridges ~~could~~can still ~~probably~~ interact with adjacent plumes under the appropriate conditions. In the case of very short ~~off-axis distance~~plume-ridge distances, there is good evidence of plume-ridge interaction in the southern ~~EPR (Conder et al., 2002; Toomey et al., 2002; Vlastélic and Dosso, 2005). But generally, the rapid movement of plate is not helpful to the ridge suction. Chances are that ridge with high velocity will drag away rather than suck plume strongly.~~Pacific ocean (e.g., Louisville plume; Conder et al., 2002; Toomey et al., 2002; Vlastélic and Dosso, 2005). Based on a series of numerical modeling as well as geological and geophysical observations, we ~~predict~~conclude that mantle plumes in the Pacific ~~Ocean~~ are more likely to ~~be dragged away by the spreading ridge~~spread away from the ridge and into the direction of plate motion than in the Atlantic and Indian Oceans. The tendency of fast plate velocities to promote plume spreading away from the MOR through viscous drag may depend, however, on the details of lithosphere-asthenosphere rheological coupling such as the presence of a weak decoupling (e.g., melt) layer (Rychert et al., 2020). Further studies of plume spreading and plume-ridge interaction are needed to shed light on the coupling of the plate-

mantle system.

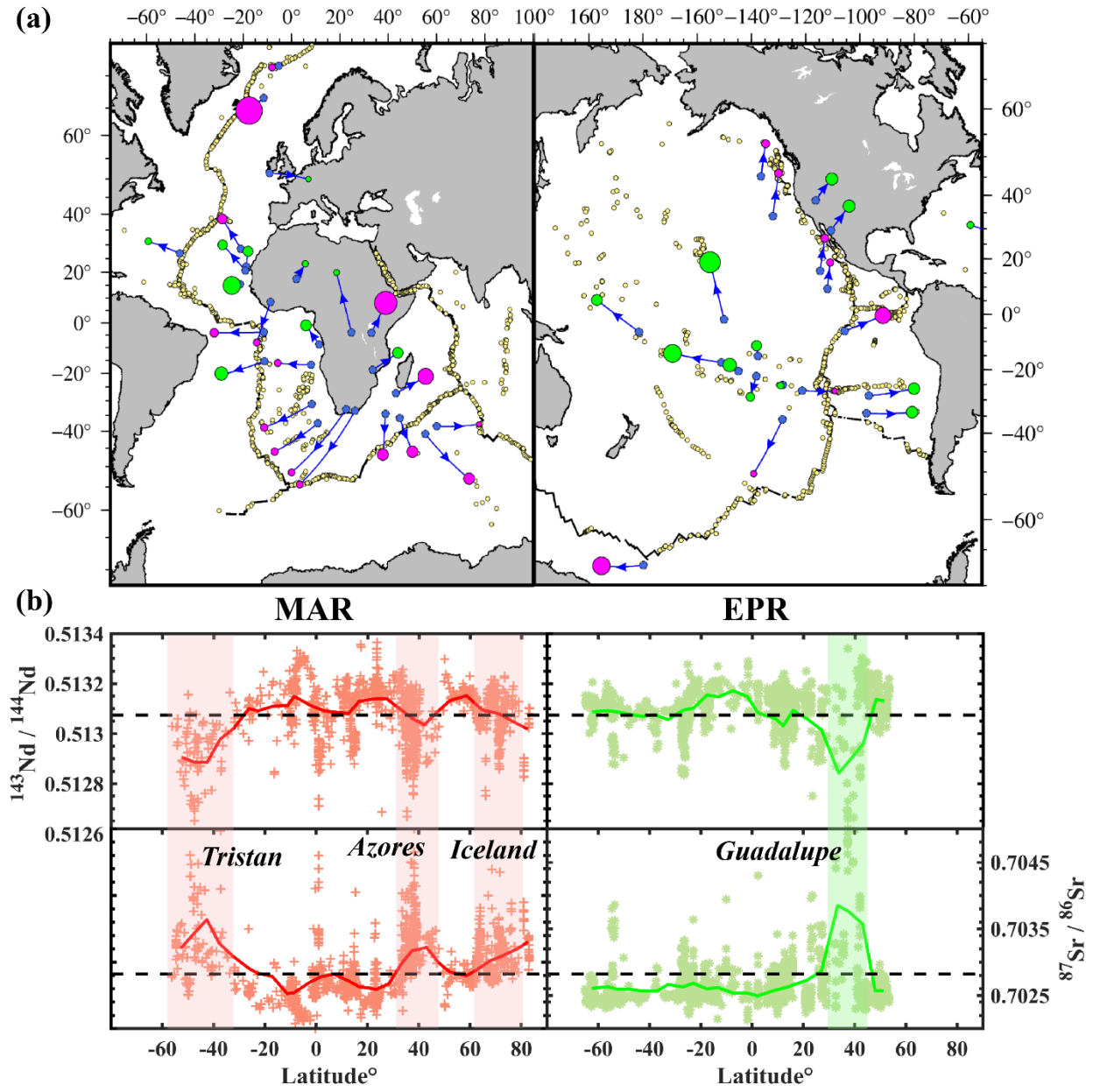

Figure 9. A compilation of hotspots along with spreading ridges in MAR and EPR. **(a)** Distribution of surface hotspots (circles) together with depth-projected source locations at CMB (blue dots) of the plumes based on (Jackson et al., 2021), using the plume catalogue of (Hoggard et al., 2020). Plumes in magenta circles are mantle plumes sucked by ridges (Ito et al., 2003), and plumes dragged away by ridges are shown as green circles, whose size refers to the plume buoyancy flux. Yellow dots are MORB samples mapped in (b). **(b)** Plot of radioactive isotopes ratios along ridge MORB samples. The

~~data are downloaded from the PetDB Database (http://portal.earthchem.org/). The colored symbols refer to samples in different mid-ocean ridge. Main hotspots influencing MORBs are labeled with shaded bands. The black dash lines are the mean MORB isotopes ratio from Gale (2013). Red and green lines are the mean ratios of the samples in MAR and EPR, respectively.~~

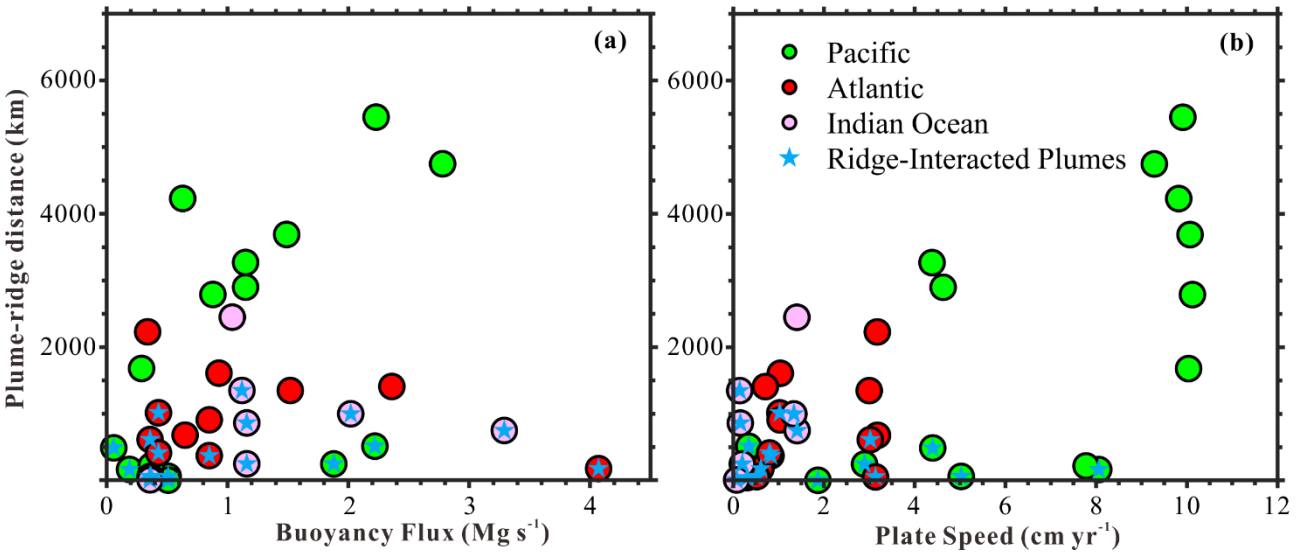

Figure 11. Buoyancy flux, plate speed and plume-ridge distance of mantle plumes in different oceans. Mantle plumes in the Pacific, Atlantic and Indian Ocean are shown in green, red and pink circles, respectively. Blue stars marked the ridge-interacted plumes according to Ito et al. (2003). **(a)** Plot of plume-ridge distance and plume buoyancy flux. Data are from Hoggard et al. (2020). **(b)** Plot of plume-ridge distance and plate speed at the location of plumes. Plume-ridge distance come from GPlates (Müller et al., 2016; Whittaker et al., 2015), and plate speed data come from Becker et al. (2015)

5 Conclusion

In this study, we explore the evolution of plume-ridge interaction with 2D thermomechanical numerical models. Based on model results, ~~following conclusions are as follows.~~we find that:

(1) Plume-ridge interaction is mainly ~~determined~~governed by the competition between the effects of

plume spreading (overpressure in the plume-head stage~~)~~), upward gravitationally-driven flow of the plume along the base of the sloping lithosphere and plate shearing~~, which is strongly influenced~~. These driving forces are controlled by plume size, plume-ridge distance and the spreading rate of the mid-ocean ridge. ~~The plume size, that is, the plume buoyancy flux, may play a critical role in controlling the connection between the two units, compared with distance and~~

~~(1)~~ MOR spreading ~~rate.~~

(2) ~~MORs can~~does not only draw upwelling plumes into the spreading center, but ~~plates~~ also ~~push~~tends to drag mantle plumes away~~. Plate-dragged mantle plumes are largely~~ from the ridge. Plume flow away from the ridge is favored by ~~week remote plume and fast~~ small and/or distant plumes as well as slow spreading ~~ridges~~rates, whereas ~~those big mantle plumes are inclined to be sucked into the~~plume flow towards the ridge is promoted by large and/or nearby plumes, as well as slow~~-~~spreading ~~MORs~~rates.

(3) ~~Mantle plumes~~ Considering the high plate velocity and typically large plume-ridge distances, mantle plumes in the Pacific ~~Ocean~~ are more likely to ~~move~~be dragged away from ~~fast-spreading~~the EPR ~~rather~~ than ~~sucked into~~being drawn towards the ridge center.

Code availability

The source numerical modeling code in this study is available from the corresponding author upon reasonable request.

Data availability

The data that support the findings of this study are available from the corresponding author upon reasonable request.

Author contribution

Fengping Pang performed all numerical models, interpreted results and wrote the manuscript. Jie Liao proposed the study, modify the code and contributed to rewriting and scientific discussion. Maxim D. Ballmer contributed with significant help in rewriting and scientific discussion. Lun Li participated in discussion and interpretations. All authors have read and edited draft versions of the paper and have approved the final version.

Competing interest

The authors declare that they have no conflict of interest.

Acknowledgement

This research is financially supported by NSFC projects (U1901214, 41974104, 91855208) and Guangdong project 2017ZT07Z066. We are grateful to Prof. Taras Gerya for his long-lasting guidance on our geodynamical modeling. We gratefully acknowledge Hongjian Fang for insightful discussions.

795 Numerical simulations were performed on the clusters of National Supercomputer Center in
796 Guangzhou (Tianhe-II).
797

Reference

Ballmer, M. D., Ito, G., Wolfe, C. J. and Solomon, S. C.: Double layering of a thermochemical plume in the upper mantle beneath Hawaii, Earth Planet. Sci. Lett., 376, 155–164, doi:10.1016/j.epsl.2013.06.022, ~~2013~~2013a.

Ballmer, M. D., Conrad, C. P., Smith, E. I. and Harmon, N.: Non-hotspot volcano chains produced by migration of shear-driven upwelling toward the East Pacific Rise, Geology, 41(4), 479–482, doi:10.1130/G33804.1, 2013b.

Ballmer, M. D., Ito, G. and Cheng, C.: Asymmetric dynamical behavior of thermochemical plumes and implications for hawaiian lava composition, Geophys. Monogr. Ser., 208, 35–57, doi:10.1002/9781118872079.ch3, 2015.

Barruol, G., Sigloch, K., Scholz, J. R., Mazzullo, A., Stutzmann, E., Montagner, J. P., Kiselev, S., Fontaine, F. R., Michon, L., Deplus, C. and Dyment, J.: Large-scale flow of Indian Ocean asthenosphere driven by Réunion plume, Nat. Geosci., 12(12), 1043–1049, doi:10.1038/s41561-019-0479-3, 2019.

Becker, T. W., Schaeffer, A. J., Lebedev, S. and Conrad, C. P.: Toward a generalized plate motion reference frame, Geophys. Res. Lett., 42(9), 3188–3196, doi:10.1002/2015GL063695, 2015.

Buff, L., Jackson, M. G., Konrad, K., Konter, J. G., Bizimis, M., Price, A., Rose-Koga, E. F., Blusztajn, J., Koppers, A. A. P. and Herrera, S.: "Missing Links" for the Long-lived Macdonald and Arago Hotspots, South Pacific Ocean, Geology, 49(5), 541–544, doi:10.1130/G48276.1, 2021.

Burov, E. and Cloetingh, S.: Erosion and rift dynamics: New thermomechanical aspects of post-rift evolution of extensional basins, Earth Planet. Sci. Lett., 150(1–2), 7–26, doi:10.1016/s0012-821x(97)00069-1, 1997.

Byerlee, J.: Friction of rocks, Pure Appl. Geophys. PAGEOPH, 116(4–5), 615–626, doi:10.1007/BF00876528, 1978.

Cheng, C., Allen, R. M., Porritt, R. W. and Ballmer, M. D.: Seismic constraints on a double-layered asymmetric whole-mantle plume beneath Hawai'i, Hawaiian Volcanoes From Source to Surf., 19–34, doi:10.1002/9781118872079.ch2, 2015.

Clouard, V. and Bonneville, A.: Ages of seamounts, islands, and plateaus on the Pacific plate, Spec. Pap. Geol. Soc. Am., 388, 71–90, doi:10.1130/0-8137-2388-4.71, 2005.

Conder, J. A., Forsyth, D. W. and Parmentier, E. M.: Asthenospheric flow and asymmetry of the East Pacific Rise, MELT area, J. Geophys. Res. Solid Earth, 107(B12), ETG 8-1-ETG 8-13, doi:10.1029/2001jb000807, 2002.

Cushman, B., Sinton, J., Ito, G. and Dixon, J. E.: Glass compositions, plume-ridge interaction, and hydrous melting along the Galapagos spreading center, 90.5 °wto 98 ° W, Geochemistry, Geophys. Geosystems, 5(8), doi:10.1029/2004GC000709, 2004.

Dalton, C. A., Langmuir, C. H. and Gale, A.: Geophysical and geochemical evidence for deep temperature variations beneath mid-ocean ridges, Science (80-.)., 344(6179), 80–83, doi:10.1126/science.1249466, 2014.

Douglass, J., Schilling, J. G. and Fontignie, D.: Plume-ridge interactions of the Discovery and Shona mantle plumes with the southern Mid-Atlantic Ridge (40°-55° S), J. Geophys. Res. Solid Earth, 104(B2), 2941–2962, doi:10.1029/98jb02642, 1999.

François, T., Koptev, A., Cloetingh, S., Burov, E. and Gerya, T.: Plume-lithosphere interactions in rifted margin tectonic settings: Inferences from thermo-mechanical modelling, Tectonophysics, 746(October 2015), 138–154, doi:10.1016/j.tecto.2017.11.027, 2018.

French, S. W. and Romanowicz, B.: Broad plumes rooted at the base of the Earth's mantle beneath major hotspots, Nature, 525(7567), 95–99, doi:10.1038/nature14876, 2015.

Gale, A., Dalton, C. A., Langmuir, C. H., Su, Y. and Schilling, J. G.: The mean composition of ocean ridge basalts, Geochemistry, Geophys. Geosystems, 14(3), 489–518, doi:10.1029/2012GC004334, 2013.

Geissler, W. H., Wintersteller, P., Maia, M., Strack, A., Kammann, J., Eagles, G., Jegen, M., Schloemer, A. and Jokat, W.: Seafloor evidence for pre-shield volcanism above the Tristan da Cunha mantle plume, Nat. Commun., (2020), doi:10.1038/s41467-020-18361-4, 2020.

Gerya, T.: Origin and models of oceanic transform faults, Tectonophysics, 522–523, 34–54, doi:10.1016/j.tecto.2011.07.006, 2012.

Gerya, T. V.: Three-dimensional thermomechanical modeling of oceanic spreading initiation and evolution, Phys. Earth Planet. Inter., 214, 35–52, doi:10.1016/j.pepi.2012.10.007, 2013.

Gerya, T. V. and Yuen, D. A.: Characteristics-based marker-in-cell method with conservative finite-differences schemes for modeling geological flows with strongly variable transport properties, Phys. Earth Planet. Inter., 140(4), 293–318, doi:10.1016/j.pepi.2003.09.006, 2003.

Gerya, T. V. and Yuen, D. A.: Robust characteristics method for modelling multiphase visco-elasto-plastic thermo-mechanical problems, Phys. Earth Planet. Inter., 163(1–4), 83–105, doi:10.1016/j.pepi.2007.04.015, 2007.

Gerya, T. V., Stern, R. J., Baes, M., Sobolev, S. V. and Whattam, S. A.: Plate tectonics on the Earth triggered by plume-induced subduction initiation, Nature, 527(7577), 221–225, doi:10.1038/nature15752, 2015.

Gülcher, A. J. P., Gerya, T. V., Montési, L. G. J. and Munch, J.: Corona structures driven by plume–

lithosphere interactions and evidence for ongoing plume activity on Venus, Nat. Geosci., 13(8), 547–554, doi:10.1038/s41561-020-0606-1, 2020.

Hardarson, B. S., Fitton, J. G., Ellam, R. M. and Pringle, M. S.: Rift relocation - A geochemical and geochronological investigation of a palaeo-rift in northwest Iceland, Earth Planet. Sci. Lett., 153(3–4), 181–196, doi:10.1016/s0012-821x(97)00145-3, 1997.

Harmon, N., Forsyth, D. W., Weeraratne, D. S., Yang, Y. and Webb, S. C.: Mantle heterogeneity and off axis volcanism on young Pacific lithosphere, Earth Planet. Sci. Lett., 311(3–4), 306–315, doi:10.1016/j.epsl.2011.09.038, 2011.

Hoggard, M. J., Parnell-turner, R. and White, N.: Hotspots and mantle plumes revisited: Towards reconciling the mantle heat transfer discrepancy, Earth Planet. Sci. Lett., 542, 116317, doi:10.1016/j.epsl.2020.116317, 2020.

Ito, G., Lin, J. and Gable, C. W.: Interaction of mantle plumes and migrating mid-ocean ridges: Implications for the Galfipagos plume-ridge system, , v, 1–3, 1997.

Ito, G., Lin, J. and Graham, D.: Observational and theoretical studies of the dynamics of mantle plume-mid-ocean ridge interaction, Rev. Geophys., 41(4), doi:10.1029/2002RG000117, 2003.

Jackson, M. G., Hart, S. R., Konter, J. G., Koppers, A. A. P., Staudigel, H., Kurz, M. D., Blusztajn, J. and Sinton, J. M.: Samoan hot spot track on a “hot spot highway”: Implications for mantle plumes and a deep Samoan mantle source, Geochemistry, Geophys. Geosystems, 11(12), doi:10.1029/2010GC003232, 2010.

Jackson, M. G., Becker, T. W.~~,~~, and Steinberger, B~~., Atlantic, P., Atlantic, P. and Pacific, L~~.: Spatial Characteristics of Recycled and Primordial Reservoirs in the Deep Mantle, Geochemistry, Geophys. Geosystems, 22(3), doi:10.1029/2020GC009525, 2021.

Jellinek, A. M., Gonnermann, H. M. and Richards, M. A.: Plume capture by divergent plate motions: Implications for the distribution of hotspots, geochemistry of mid-ocean ridge basalts, and estimates of the heat flux at the core-mantle boundary, Earth Planet. Sci. Lett., 205(3–4), 361–378, doi:10.1016/S0012-821X(02)01070-1, 2003.

Jiang, Q., Jourdan, F., Olierook, H. K. H., Merle, R. E. and Whittaker, J. M.: Longest continuously erupting large igneous province driven by plume-ridge interaction, Geology, 1–3, doi:10.1130/G47850.1, 2020.

~~Katz, R. F.~~Kincaid, C., Ito, G. and ~~Spiegelman, M.: A new parameterization~~Gable, C.: Laboratory investigation of ~~hydrous~~the interaction of off-axis mantle ~~melting, , 1–19~~plumes and spreading centres, Nature, 376(6543), 758–761, doi:10.~~1029/2002GC000433, 2003~~1038/376758a0, 1995.

Kincaid, C., Schilling, J.-G. and Gable, C.: The dynamics of off-axis plume-ridge interaction in the uppermost mantle, Earth Planet. Sci. Lett., 137(1–4), 29–43, doi:10.1016/0012-821X(95)00201-M, 1996.

~~Koptev, A., Calais, E., Burov, E., Leroy, S. and Gerya, T.: Dual continental rift systems generated by plume-lithosphere interaction, Nat. Geosci., 8(5), 388–392, doi:10.1038/ngeo2401, 2015.~~

Koppers, A. A. P., Becker, T. W., Jackson, M. G., Konrad, K., Müller, R. D., Romanowicz, B., Steinberger, B. and Whittaker, J. M.: Mantle plumes and their role in Earth processes, Nat. Rev. Earth Environ., 2(6), 382–401, doi:10.1038/s43017-021-00168-6, 2021.

Lénat, J. F., Merle, O. and Lespagnol, L.: La réunion: An example of channeled hot spot plume, J. Volcanol. Geotherm. Res., 184(1–2), 1–13, doi:10.1016/j.jvolgeores.2008.12.001, 2009.

~~Li, A. and Detrick, R. S.: Azimuthal anisotropy and phase velocity beneath Iceland: Implication for plume-ridge interaction, Earth Planet. Sci. Lett., 214(1–2), 153–165, doi:10.1016/S0012-~~

~~821X(03)00382-0, 2003.~~

Maia, M., Pessanha, I., Courrges, E., Patriat, M., Gente, P., Hémond, C., Janin, M., Johnson, K., Roest, W., Royer, J. Y. and Vatteville, J.: Building of the Amsterdam-Saint Paul plateau: A 10 Myr history of a ridge-hot spot interaction and variations in the strength of the hot spot source, J. Geophys. Res. Solid Earth, 116(9), 1–19, doi:10.1029/2010JB007768, 2011.

Mittelstaedt, E., Ito, G. and Behn, M. D.: Mid-ocean ridge jumps associated with hotspot magmatism, Earth Planet. Sci. Lett., 266(3–4), 256–270, doi:10.1016/j.epsl.2007.10.055, 2008.

Mittelstaedt, E., Ito, G. and Van Hunen, J.: Repeat ridge jumps associated with plume-ridge interaction, melt transport, and ridge migration, J. Geophys. Res. Solid Earth, 116(1), 1–20, doi:10.1029/2010JB007504, 2011.

Mittelstaedt, E., Soule, S., Harpp, K., Fornari, D., McKee, C., Tivey, M., Geist, D., Kurz, M. D., Sinton, C. and Mello, C.: Multiple expressions of plume-ridge interaction in the Galápagos: Volcanic lineaments and ridge jumps, Geochemistry, Geophys. Geosystems, 13(5), doi:10.1029/2012GC004093, 2012.

Montelli, R., Nolet, G., Dahlen, F. A., Masters, G., Engdahl, E. R. and Hung, S. H.: Supporting OnlineMaterial Timing, Science, 303(5656), 338–343, doi:10.1126/science.1092485, 2004.

Morgan, W. J.~~: Convection plumes in the lower mantle, Nature, 230(5288), 42–43, doi:10.1038/230042a0, 1971~~: Rodriguez, Darwin, Amsterdam, ..., A second type of Hotspot Island, J. Geophys. Res. Solid Earth, 83(8), 5355–5360, 1978.

Müller, R. D., Roest, W. R. and Royer, J.-Y.: Asymmetric sea-floor spreading caused by ridge–plume interactions, Nature, 396(6710), 455–459, doi:10.1038/24850, 1998.

Müller, R. D., Seton, M., Zahirovic, S., Williams, S. E., Matthews, K. J., Wright, N. M., Shephard,

G. E., Maloney, K. T., Barnett-Moore, N., Hosseinpour, M., Bower, D. J. and Cannon, J.: Ocean Basin Evolution and Global-Scale Plate Reorganization Events since Pangea Breakup, Annu. Rev. Earth Planet. Sci., 44, 107–138, doi:10.1146/annurev-earth-060115-012211, 2016.

Niu, Y.: Ridge suction drives plume-ridge interactions, , (October), doi:10.13140/2.1.4728.0961, 2014.

O'Connor, J. M., Jokat, W., Le Roex, A. P., Class, C., Wijbrans, J. R., Keßling, S., Kuiper, K. F. and Nebel, O.: Hotspot trails in the South Atlantic controlled by plume and plate tectonic processes, Nat. Geosci., 5(10), 735–738, doi:10.1038/ngeo1583, 2012.

Ranalli: Rheology of the Earth, 1995.

Ribe, N. M.: The dynamics of plume-ridge interaction: 2. Off-ridge plumes, , 101, 1996.

Ribe, N. M. and Christensen, U. R.: Three-dimensional modeling of plume-lithosphere interaction, , 99, 669–682, 1994.

Ribe, N. M. and Christensen, U. R.: The dynamical origin of Hawaiian volcanism, Earth Planet. Sci. Lett., 171(4), 517–531, doi:10.1016/S0012-821X(99)00179-X, 1999.

Ribe, N. M., Christensen, U. R. and Theißing, J.: The dynamics of plume-ridge interaction, 1: Ridge-centered plumes, Earth Planet. Sci. Lett., 134(1–2), 155–168, doi:10.1016/0012-821X(95)00116-T, 1995.

Rowley, D. B. and Forte, A. M.: Kinematics of the East Pacific Rise Retrodicted From Pacific and Farallon/Nazca Subduction-Related Torques: Support for Significant Deep Mantle Buoyancy Controlling EPR Spreading, J. Geophys. Res. Solid Earth, 127(2), 1–24, doi:10.1029/2020JB021638, 2022.

Rowley, D. B., Forte, A. M., Rowan, C. J., Glišović, P., Moucha, R., Grand, S. P. and Simmons, N.

A.: Kinematics and dynamics of the east pacific rise linked to a stable, deep-mantle upwelling, Sci. Adv., 2(12), 1–19, doi:10.1126/sciadv.1601107, 2016.

Rychert, C. A., Harmon, N., Constable, S. and Wang, S.: The Nature of the Lithosphere-Asthenosphere Boundary, J. Geophys. Res. Solid Earth, 125(10), 1–39, doi:10.1029/2018JB016463, 2020.

Schilling, J. G.: Fluxes and excess temperatures of mantle plumes inferred from their interaction with migrating mid-ocean ridges, Nature, 352(6334), 397–403, doi:10.1038/352397a0, 1991.

Sleep, N. H.: Lateral flow and ponding of starting plume material, J. Geophys. Res. Solid Earth, 102(B5), 10001–10012, doi:10.1029/97jb00551, 1997.

Small, C.: Observations of ridge-hotspot interactions in the Southern Ocean, J. Geophys. Res., 100(B9), doi:10.1029/95jb01377, 1995.

Straume, E. O., Gaina, C., Medvedev, S., Hochmuth, K., Gohl, K., Whittaker, J. M., Abdul Fattah, R., Doornenbal, J. C. and Hopper, J. R.: GlobSed: Updated Total Sediment Thickness in the World's Oceans, Geochemistry, Geophys. Geosystems, 20(4), 1756–1772, doi:10.1029/2018GC008115, 2019.

Toomey, D. R., Wilcock, W. S. D., Conder, J. A., Forsyth, D. W., Blundy, J. D., Parmentier, E. M. and Hammond, W. C.: Asymmetric mantle dynamics in the MELT region of the East Pacific Rise, Earth Planet. Sci. Lett., 200(3–4), 287–295, doi:10.1016/S0012-821X(02)00655-6, 2002.

Torsvik, T. H., Smethurst, M. A., Burke, K. and Steinberger, B.: Large igneous provinces generated from the margins of the large low-velocity provinces in the deep mantle, Geophys. J. Int., 167(3), 1447–1460, doi:10.1111/j.1365-246X.2006.03158.x, 2006.

Turcotte, D. and Schubert, G.: Geodynamics, Cambridge University Press., 2014.

Vlastélic, I. and Dosso, L.: Initiation of a plume-ridge interaction in the South Pacific recorded by high-precision Pb isotopes along Hollister Ridge, Geochemistry, Geophys. Geosystems, 6(5), 1–13, doi:10.1029/2004GC000902, 2005.

Whittaker, J. M., Afonso, J. C., Masterton, S., Müller, R. D., Wessel, P., Williams, S. E. and Seton, M.: Long-term interaction between mid-ocean ridges and mantle plumes, Nat. Geosci., 8(6), doi:10.1038/NGEO2437, 2015.

Wolfe, C. J., Solomon, S. C., Laske, G., Collins, J. A., Detrick, R. S., Orcutt, J. A., Bercovici, D. and Hauri, E. H.: Mantle shear-wave velocity structure beneath the Hawaiian hot spot, Science (80-.)., 326(5958), 1388–1390, doi:10.1126/science.1180165, 2009.

Yang, A. Y., Zhao, T. P., Zhou, M. F. and Deng, X. G.: Isotopically enriched N-MORB: A new geochemical signature of off-axis plume-ridge interaction—A case study at 50°28′E, Southwest Indian Ridge, J. Geophys. Res. Solid Earth, 122(1), 191–213, doi:10.1002/2016JB013284, 2017.